

Matiss Malahs

Design of a Low Cost Laser Vibrometer System

Helsinki Metropolia University of Applied Sciences

Bachelor of Engineering

Electronics

Thesis

March 2015

Author Title	Matiss Malahs Design of a Low Cost Laser Vibrometer System
Number of Pages Date	37 pages + 11 appendices 26 March 2015
Degree	Bachelor of Engineering
Degree Programme	Electronics
Instructor	Kai Lindgren, Senior Lecturer
<p>The aim of this study was to develop a functional low cost laser vibrometer system capable of measuring the vibrational frequency of an object. The thesis explains the underlying operational principles of commercially available laser vibrometers, and based on the research a functional system is developed.</p> <p>The development of the system consisted of three main parts - sensor part, analog signal analysis and digital signal processing. In the study emphasis was put on the development of the sensor part and analog signal analysis, while the digital signal processing was done using "NI myDaq" hardware and "LabView" software. The system design was divided into smaller subsections where the design of each part of the system was analysed and discussed in more detail.</p> <p>An operational system capable of detecting vibrational frequency of an object with a laser beam was developed, thus fulfilling the objective of thesis. The system was thoroughly tested in several measurement setups to determine the operational limits and maximum detectable vibrational frequency. While there is a number of possible future improvements and additional tests should be carried out, the system is fully capable of detecting vibration of an object remotely and non-intrusively.</p>	
Keywords	Laser Vibrometer, Laser Doppler Vibrometer

Contents

1	Introduction	1
2	Theory and Operation	2
2.1	Characterization and History	2
2.2	Interferometry	3
2.2.1	Interference of Light	3
2.2.2	Michelson Interferometer	4
2.2.3	Fabry-Perot Interferometer	5
2.3	Laser Doppler Vibrometer	6
2.3.1	Doppler Effect	6
2.3.2	Operation Principle	7
2.4	Grazing Laser Vibrometer	9
2.5	Laser Classification and Safety	10
3	System Design	12
3.1	Laser and Photodiode	12
3.2	Transimpedance Amplifier Design	14
3.2.1	Theory and Design	14
3.2.2	Measurements	16
3.2.3	Simulation	17
3.3	Filter Design	18
3.3.1	Theory and Design	18
3.3.2	Measurements and Simulation	21
3.4	Level Shifter	21
3.4.1	Theory and Design	21
3.4.2	Simulation and Measurements	23
3.5	Voltage Rail Splitter	24
3.6	Component Selection	26
3.7	Printed Circuit Board Design	27
4	Measurements Results and Suggestions	28
4.1	Measurement Results	28
4.2	Flow Diagram of GLV System	32
5	Conclusion and Discussion	34

Appendices

Appendix 1. Laser

Appendix 2. Measurement Setup

Appendix 3. Frequency Response of TIA Simulation

Appendix 4. Frequency and Phase Response of Theoretical and Factual Low-pass Filter Simulation

Appendix 5. Frequency and Phase Response of Theoretical and Factual High-pass Filter Simulation

Appendix 6. Input and Output Voltage of Simulated Level Shifter Circuit

Appendix 7. Circuit Diagram of the Main Board

Appendix 8. PCB Layout of the Main Board

Appendix 9. Theoretical Frequency Response of the Whole Systems Simulation

Appendix 10. Block Diagram of LabVIEW Program

Appendix 11. Measurement Values of Figure 16

Abbreviations

MEMS	Micro-electro-mechanical system
MOEMS	Micro-opto-electro-mechanical system
λ	Wavelength
φ	Phase shift
LDV	Laser Doppler vibrometer
DUT	Device under test
GLV	Grazing laser vibrometer
IR	Infrared
PD	Photodiode
$f_{-3\text{dB}}$	-3dB corner frequency
C_F	Feedback capacitor
SR	Slew rate
ADC	Analog to digital converter
TIA	Transimpedance amplifier

1 Introduction

Laser vibrometry nowadays is widely used in many application fields like automotive industry, quality and process control, civil engineering, and many others. In laser vibrometry, as the name suggests, the measurement of vibration is carried out using a laser beam, thus enabling non-contact, non-intrusive remote vibration measurements. Depending on the application and complexity, the price of these systems can reach tens of thousands of euros.

The aim of this thesis is to develop and design a low cost laser vibrometer system that would enable remote vibrational frequency detection of a vibrating object. The scope of this thesis includes the examination of the underlying operational principles and phenomena of laser vibrometers that are available on the market, as well as a thorough explanation and analysis of the developed system.

Ultimately an operating laser vibrometer system is developed and scrutinized in the extent of this thesis. A final printed circuit board is produced based on the research and design considerations introduced in this document. Finally, complete test arrangement, operational characteristics, and test results of the system are presented.

2 Theory and Operation

2.1 Characterization and History

Laser vibrometry is a method used for non-contact vibration measurements. As the measurement made with a laser vibrometer is non-intrusive and non-destructive it has many fields of application. Applications include automotive industry, architecture, aerospace, security and many others. One of the first inventions in laser vibrometry application in security would be the “Buran” eavesdropping system created by a Soviet inventor Leon Theremin for which he received the First Class Stalin Prize. This system used an infrared laser to covertly detect speech from a window of a room in which people were conversing. It is believed that the system was used to eavesdrop on American and French embassies as well as Stalin himself. It is considered that this system is the original predecessor of the modern laser microphones. [1]

Nowadays there are several companies like “Polytec” or “OMS Corporation” producing refined laser vibrometers for a range of applications. The detectable vibrational frequency range is from DC or 0 Hz up to 1.2 GHz for the most advanced systems. Depending on the application, the necessary system with the appropriate frequency range can be chosen. Low frequency measurements are widely used to test and monitor engines and motors as well as it is used in structural integrity testing whereas high frequency measurements are used in micro system analysis like micro-electro-mechanical system (MEMS) or micro-opto-electro-mechanical system (MOEMS) testing [2]. Some companies specialize in production and distribution of laser microphones. Though it must be noted that, as this kind of device can be used to secretly eavesdrop on conversations thus breaking a person’s privacy, some of the distributors sell their systems only to law enforcement and government agencies [3].

The fundamental operational principle of a laser vibrometer is that the vibrational frequency of a surface can be measured by analysing the reflected laser beam from the investigated surface. Depending on the desired measurable frequency range, resolution, and sensitivity, the complexity of the system can vary from a very simple, small sized device with few components to a sophisticated system capable of distinguishing minute changes in vibrational frequency. Two main physical phenomena that give rise to the

possibility of detecting vibrations at very high frequencies with great sensitivity are interference and Doppler Effect. These phenomena and their application in laser vibrometry are discussed in the following chapters.

2.2 Interferometry

2.2.1 Interference of Light

Interference of light is described as the interaction of two or more light sources. The sources of light must be coherent - the light waves must have equal frequencies and unchanging phase difference over time. As the laser light is monochromatic light with specific frequency it can be used to obtain interference patterns, whereas, for example, the light from incandescent light bulb could not be used, as it is composed of many frequency components. Superposition principle is used to describe wave interference. If two or more coherent light waves go past a specified point, their amplitudes at that point are added or subtracted depending on phase of the waves. If the phases are equal the amplitudes are added and if the phases are opposite than the amplitudes are subtracted. Constructive interference can be observed when the phases of the waves are equal and destructive interference when the phases are opposite. At any other point than the previously mentioned situations, partial cancellation interference can be detected. The interference pattern of two coherent waves is represented in Figure 1.

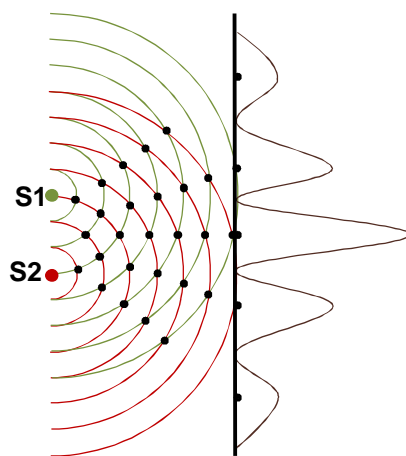


Figure 1. Representation of an interference pattern produced by two sources of waves.

Physically this kind of demonstration can be done using one monochromatic light source and a panel with two slits. If a screen is placed behind the panel with two slits the interference pattern as shown in Figure 1 can be observed. English physicist Thomas Young was the first person to demonstrate this double slit experiment in 1801 [4,25].

2.2.2 Michelson Interferometer

A device called Michelson interferometer is used to produce interference fringes from a beam of monochromatic light that is split into two parts. Afterwards, by bringing the split beam of light back together on a screen or a photodetector, interference pattern can be observed. In Figure 2 the schematic illustration of the Michelson interferometer is shown.

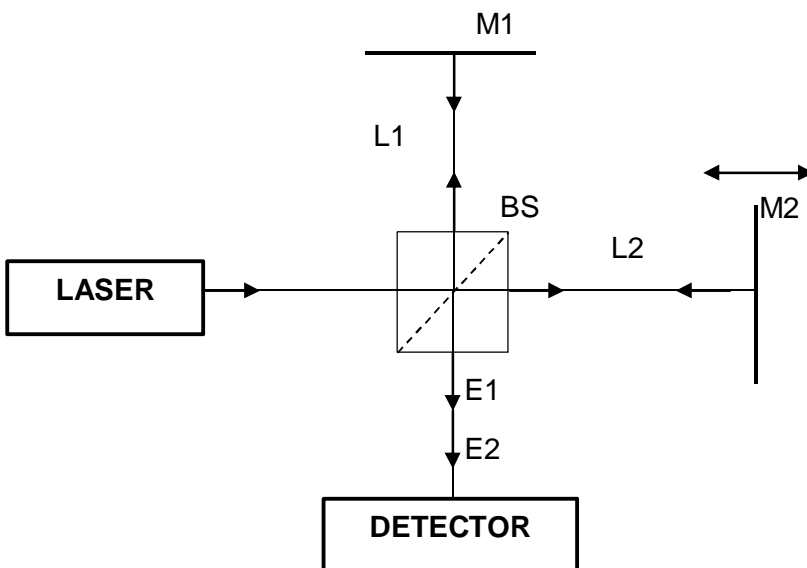


Figure 2. Simplified schematic of Michelson interferometer.

In this schematic the laser light or other monochromatic light is split into two parts by the beam splitter in the schematic denoted as BS. One part of the split light beam is refracted in the direction of the static mirror denoted as M1, while the other part travels towards adjustable mirror M2. When both of the light beams are reflected from the mirrors they are again combined in the beam splitter and travel in the direction of the detector where the interference pattern is detected. The interference pattern depends on the difference of the path lengths that the split beams have to travel. [5,163-165.] By changing the position of the second mirror the interference pattern on the detector will change. By knowing the number of interference fringes it is possible to derive the distance by which the second mirror was moved using equation (1), where λ is the wavelength of the used

light, n is the number of fringes, x_1 is the initial position of the second mirror and x_2 is the final position. [6,106.]

$$\begin{aligned} 2(x_2 - x_1) &= n\lambda \\ (x_2 - x_1) &= \frac{n\lambda}{2} \end{aligned} \quad (1)$$

2.2.3 Fabry-Perot Interferometer

A Fabry-Perot interferometer in its most simple configuration consists of two semi-reflective mirrors placed in parallel to each other. The thickness of the mirrors is negligible and the distance between the mirrors usually ranges from micrometres to several centimetres. The basic configuration of a Fabry-Perot interferometer is shown in figure 3. M1 is the static mirror, M2 is the movable mirror, and L represents the distance between the mirrors.

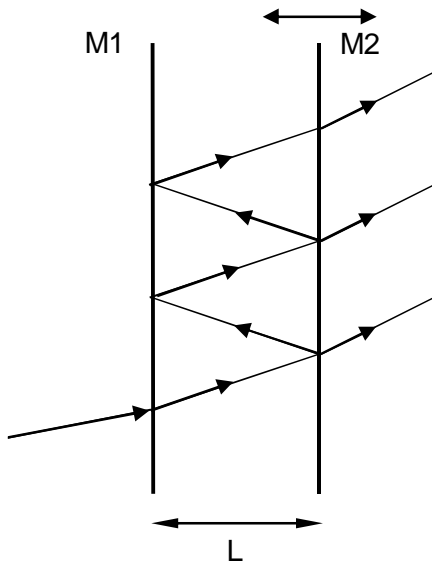


Figure 3. Schematic of wave propagation in Fabry-Perot interferometer.

An incident wave on the first mirror is partially reflected and partially refracted depending on the reflectivity of the mirror. When the refracted wave reaches the second mirror it is again partially reflected and refracted. All of the refracted waves interfere with each other infinitely creating a specific interference pattern. The phase difference between two subsequent sets of refracted waves is given by equation (2).

$$\varphi = 2\pi \left(\frac{2L}{\lambda} \right) \quad (2)$$

Every time the phase difference is equal to an integer of 2π a resonance condition is met, which means that maximum of transmission is reached. In equation (3) resonance condition is expressed with q being an integer.

$$q = \frac{2L}{\lambda} \quad (3)$$

As shown in equation (4) the frequency separation between two adjacent interference modes can be derived and by using this formula the distance between the mirrors can be determined [7,256].

$$\begin{aligned} v &= q \left(\frac{c}{2L} \right), \\ \Delta v &= \frac{c}{2L} (q + 1) - \frac{c}{2L} q = \frac{c}{2L}, \\ L &= \frac{c}{2\Delta v}. \end{aligned} \quad (4)$$

2.3 Laser Doppler Vibrometer

Laser Doppler vibrometer (LDV) is a device that measures vibration of a surface of an object by manipulating and analysing the reflected laser beam from the object. To make the measurement possible interferometry as well, as the name of the device implies, Doppler Effect are applied. Measurement done with a LDV is non-intrusive, non-destructive, creates no mass loading on the measured object, and is relatively precise and sensitive. Because of the previously mentioned reasons it is applied in many fields like medicine, automation, architecture, production of electronics and many other.

2.3.1 Doppler Effect

Doppler Effect is a phenomenon describing the change of frequency of an observed source of waves that is moving relative to the observer. The phenomenon applies to electromagnetic as well as mechanical waves. The frequency appears to be higher if the observer and source are moving towards each other and lower if they are moving away from each other, as shown in equation (5), where v_w is the propagation velocity of the wave in the given medium, v_o is the velocity of the observer relative to the medium, v_s is the velocity of the source relative to the medium, f_s is the emitted frequency of the source, and f_D is the observed Doppler shifted frequency. If the distance between the observer and source is decreasing then the first formula of equation (5) is used and if the distance is increasing then the second formula of equation (5) is used. Einstein's Special Relativity

suggests that the Lorentz Transformation must be introduced if the speed of wave approaches the speed of light, but, as the measurements are done in the same reference frame, Lorentz Transformation can be neglected [8,4].

$$\begin{aligned} f_D &= \left(\frac{v_w + v_o}{v_w - v_s} \right) f_s \\ f_D &= \left(\frac{v_w - v_o}{v_w + v_s} \right) f_s \end{aligned} \quad (5)$$

It must be noted that the velocity of the source and observer are relative to the medium where the waves propagate. Therefore for waves like sound waves, which necessitate a medium for propagation, the velocity and direction of the medium must be taken into account. This is not the case with light as it does not require a medium for propagation, consequently in calculations of Doppler shift of a light source only the velocities and directions of the source and observer must be taken into account. [8,2-3.]

2.3.2 Operation Principle

To detect the vibration of an object Doppler Effect is applied. If a laser beam is focused on the device under test (DUT) and DUT is moving with a certain speed, then the reflected laser beam frequency will be shifted as explained previously. By knowing the speed of vibration the vibrational frequency can be derived. Usually the output of an LDV is an analog voltage that is directly proportional to the speed and frequency of the vibration. To extract the Doppler shift frequency, which correlates with the speed of the vibration, interferometry is used. For example, Michelson Interferometer or some kind of modification of it can be used to detect the Doppler shift frequency. Looking back at figure 2 let us consider that mirror 2 is the DUT vibrating at certain frequency. As the DUT will be moving back and forth it will introduce a Doppler shift in the reflected laser beam, thus changing its frequency. Afterwards the reflected beam will be superimposed with the original reference beam in the beam splitter and will produce a changing interference pattern on the detector which will vary depending on the vibration of the DUT. The vibrational information afterwards can be extracted from the interference pattern either by measuring the distance between the produced interference fringes or by measuring the intensity of the light. A LDV in Fabry-Perot configuration could as well be used in the same application, as it is possible to extract the necessary information to detect the vibrational speed and frequency.

The basic operation of a practical LDV will be discussed more in detail in the following section. This is only one example of a setup as different setups are possible. The LDV optical configuration is shown in figure 4, here M stands for mirror, BS for beam splitter, BC for Bragg cell, and O is the object.

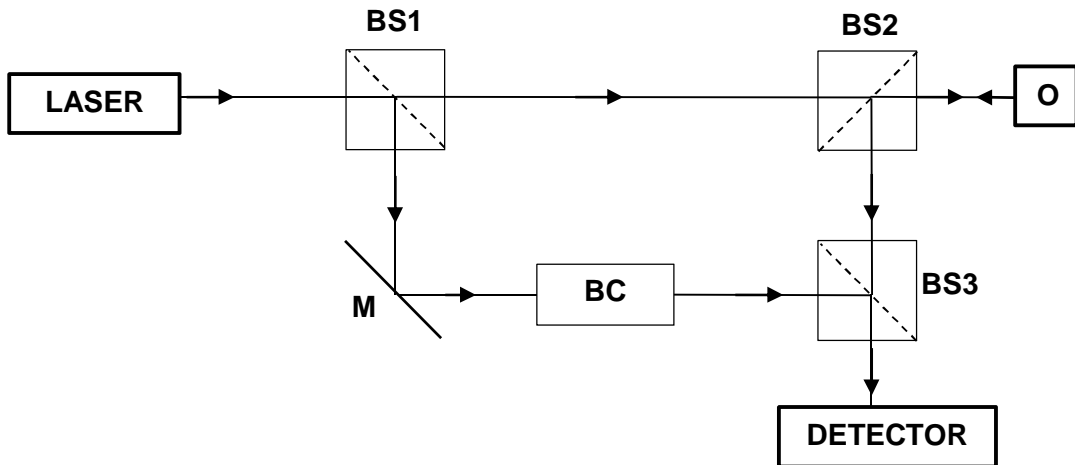


Figure 4. Simplified setup of Laser Doppler vibrometer.

Monochromatic light produced by the laser is split into two parts by the first beam splitter. The reference beam is directed towards the Bragg cell while the other part of the light after passing second beam splitter is directed on the object. The reflected beam is deflected towards the third beam splitter where it is superimposed with the reference beam and directed to the detector where an interference pattern is produced according to the objects movement. The total intensity falling on the detector can be expressed, as shown in equation (6), where r_1 denotes the optical path length of the reference beam, r_2 is the optical path length of the test beam, and λ is the wavelength of the laser beam.

$$I = I_1 + I_2 + 2\sqrt{I_1 I_2} \cos\left[\frac{2\pi(r_1 - r_2)}{\lambda}\right] \quad (6)$$

In equation (6) the third term of the intensity sum is interference term which describes the intensity change produced by the difference in the path lengths of test beam and reference beam.

The Bragg cell shown in figure 4 is an acousto-optic modulator which shifts the laser light frequency by much lower frequency in the MHz range. If the modulating frequency of the Bragg cell is 40 MHz then a fringe pattern of 40 MHz will be produced on the detector. Without a Bragg cell it would not be possible to detect the direction of the movement of the sample as the interference pattern would be the same for both movement directions.

If the information about the direction in which the object is moving is not necessary, the Bragg cell can be omitted. [9.]

2.4 Grazing Laser Vibrometer

In this section the operational principles of a grazing laser vibrometer (GLV) will be explained. Based on this principle a vibration measurement system was developed and is thoroughly discussed in the following chapters. Even though this kind of system is less sensitive and the detectable frequency range is much lower than interferometric laser vibrometers, it is considerably cheaper and smaller and could be used in applications where the precision is not of the highest importance. For example, one application field would be continuous vibration monitoring of motors, where it is important to detect the moment when the motor is starting to fail so it could be repaired before a complete failure.

The operational basis of a GLV is much simpler than that of an interferometric vibrometer. As shown in figure 5 it consists of two main parts - the laser and the detector.

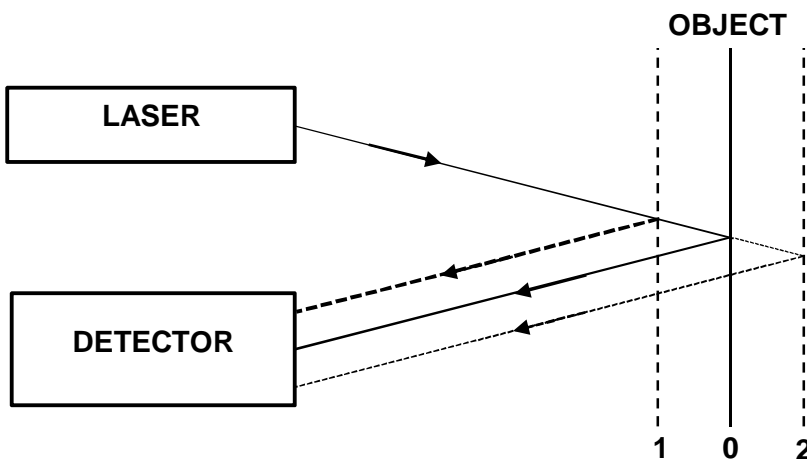


Figure 5. Schematic of a grazing laser vibrometer.

The laser beam is directed on to the vibrating object and the reflection is gathered by the detector. The underlying concept of how the vibration frequency of the object is detected is different than that which is applied in LDV. While LDV detects the frequency by detecting the velocity of movement by Doppler Effect, GLV detects the intensity changes in the reflected laser beam introduced by the vibrating object. When the object is deflected away from laser (position 2 in figure 5), the distance the laser beam must travel becomes larger. Therefore laser beam intensity that returns to detector is smaller and vice versa

when the object is deflected towards the laser (position 1 in figure 5). The change in laser beam intensity is caused by the inverse square law, which states that the intensity or irradiance of a light source is inversely proportional to square of the distance it has travelled. The square law is shown in equation (7), where I stands for intensity of light and d stands for distance.

$$I \propto \frac{1}{d^2} \quad (7)$$

Another thing that must be noted is that the position of the reflection on the detector also changes with changing deflection, as shown in figure 5. For detectors that do not have a constant sensitivity over the whole area, it must be taken into account that there will be some inconsistencies because of the position change of the reflected laser beam on the detector. Immediately one major drawback of this system can be seen from the arrangement in figure 5. As the distance between the detector and object is increased it becomes more complicated to aim and direct the reflected beam onto the detector surface. But at small distances, not exceeding one meter, the alignment process is comparatively simple and fast.

The main differences between a GLV and LDV are sensitivity, detectable frequency range, resolution, and price. Advanced LDV systems that are available on the market can have amplitude resolution of 1.5 pm and maximum vibration frequency as high as 1.2 GHz [10]. As well the price of such systems reaches as high as tens of thousands of euros. After reviewing the available devices on the market, it was visible that none of them apply the principle of previously described GLV and even the cheapest LDV systems cost in the range of thousands of euros. As will be shown in the following part of this thesis, it is possible to develop a simple low-cost vibration measurement system based on GLV operational principle.

2.5 Laser Classification and Safety

The laser used in vibrometry must produce a stable monochromatic light for the measurements. There are three main types of lasers: semiconductor type lasers, solid-state lasers, and gas lasers. In metrology general solid-state and gas lasers have been used more widely as they produce more stable and reliable light beam, but, with developments in semiconductor technology, semiconductor lasers are being used more. An example of a prominent widely used gas laser is He-Ne laser which produces coherent light at wavelength of 632.8 nm.

Lasers are classified in 4 main groups. Class 1 includes lasers that do not produce any risk for eyes or skin. Class 1M is defined so that the laser has no risk harming the skin or naked eye. Eye injury is possible if the laser beam is viewed through eye loupes or binoculars. Class 2 specifies that the laser light in the visible spectrum has no risk to skin and no risk to eyes for short time exposure. The maximum output power of class 2 lasers must be smaller than 1 mW. Similarly to Class 1M, Class 2M laser has no risk harming the skin or naked eye for short time exposure. Class 3R lasers are specified as to create no risk to skin and low risk to eyes with power limit up to 5 mW, whereas Class3B lasers have low risk to skin and medium to high risk to eyes with power limit of 500 mW. Finally Class 4 lasers have high risk to eyes and skin and output power exceeds 500 mW.

[11,225-227.]

When designing a system which uses a laser that is not enclosed in a casing the maximum output power of the laser must be carefully considered, as improper design may lead to lasting health damage. The lasers used in LDV systems available on the market essentially do not exceed 5 mW output power and can be used without particular caution.

3 System Design

3.1 Laser and Photodiode

The laser that was chosen for the system is a semiconductor laser diode that has wavelength of 650 nm which corresponds to red light. A visible spectrum laser, not an infrared (IR) laser, was used to simplify the targeting process as it would be comparatively difficult to focus the laser beam on the detector, if it was not visible. The lasers maximum output power is 5 mW at 3 V and the current consumption at that voltage is 10 mA. By the previously described classification of lasers this laser can be classified as 3R. The outer diameter of the laser casing is 6 mm, inner diameter is 3 mm, and length is 13 mm. A picture of the laser is shown in appendix 1. The specification of the laser does not state the divergence of the laser beam, but it indicates that the spot size is 10 - 15 mm at distance of 15 m. Using these values the beam divergence was calculated to be in the range from 0.47 mrad to 0.8 mrad as shown in equation (8). In this equation D_1 and D_2 denotes the diameter of the beam at two positions and L is the distance between these points.

$$\theta = 2 \arctan\left(\frac{D_2 - D_1}{2L}\right) \quad (8)$$

Divergence of the laser is comparatively low as high-end He-Ne lasers typically have divergence of 0.5 mrad to 3 mrad [12,76].

A control for the laser diodes brightness was designed and the schematic drawing is shown in figure 6. The supply voltage of the circuit is 9 V and the resistor values correspond to the ones shown in figure 6.

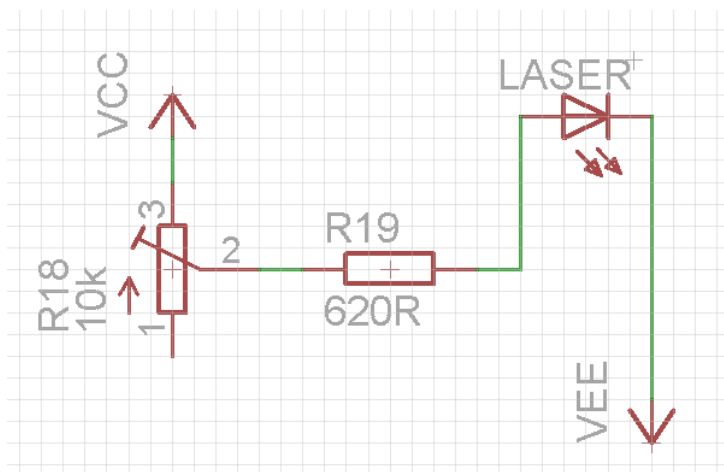


Figure 6. Circuit schematic of laser brightness control.

The circuit shown in figure 6 uses a simple voltage divider to control the current, thus the brightness of the laser. The $620\ \Omega$ resistor is used to limit the maximum current to the lasers maximum current rating which is approximately 10 mA and the potentiometer then increases the resistance of the circuit, hence decreases the current and brightness of the laser. The calculations of the circuit are shown in equation (9).

$$R_{19} = \frac{U_s - U_L}{I_{max}} = \frac{9-3}{10*10^{-3}} = 600\Omega \sim 620\Omega \quad (9)$$

U_s is voltage supply, U_L is the voltage drop across the laser diode, and I_{max} denotes lasers maximum current rating. By calculation the resistor value should be $600\ \Omega$, but a $620\ \Omega$ resistor was used as it is the closest value of the available standard resistor values.

To detect the changes introduced in the reflected laser beam BPW34 photodiode was used. It is a silicon PIN photodiode which has high speed and high radiant sensitivity and it is used in near infrared and visible light applications. Photodiode converts light into current because of the photoelectric effect. Figure 7 shows the relative spectral sensitivity of the photodiode in relation to the wavelength of the light.

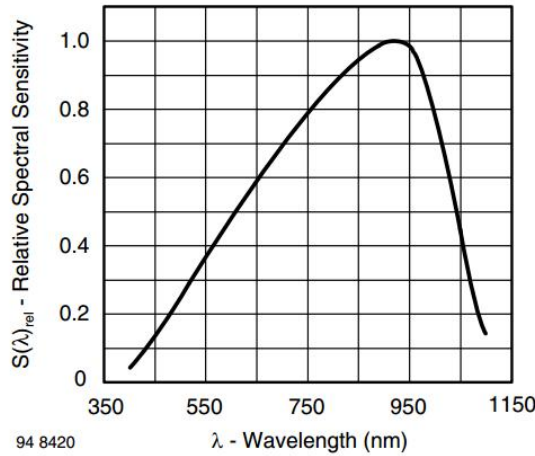


Figure 7. Relative spectral sensitivity vs. wavelength for BPW34 [13,3].

As shown in figure 7 the maximum sensitivity is reached at 900 nm range, which corresponds to infrared light. At wavelength of 650 nm , which corresponds to the wavelength of the laser that is used, the sensitivity is 0.6. Another reason why this photodiode is preferable for the application is its wide angle of sensitivity. As specified in the datasheet the angle of half sensitivity is as high as $\pm 65^\circ$ and the radiant sensitive area of the sensor is 7.5 mm^2 . The wide angle of sensitivity simplifies the aiming process as the reflected

laser beam can fall onto the photodiode from a comparatively wide angle. The diode capacitance C_{PD} is 70 pF. [13.]

3.2 Transimpedance Amplifier Design

Transimpedance amplifier (TIA) also called current to voltage or I/U converter is an operational amplifier (op amp) circuit which, as the name of the circuit suggests, converts current to voltage. The output voltage of the circuit is proportional to the input current. This circuit is used in applications where a small current, for example, a current from a sensor must be converted into a voltage.

3.2.1 Theory and Design

In this design TIA will be used to convert the photodiode's generated current into voltage. The circuit is similar to an op amp integrator and is shown in figure 8. In the circuit diagram R_F is feedback resistor, C_F - feedback capacitor, PD - photodiode, C_{PD} - photodiodes internal capacitance, and C_{IN} - input capacitance of the operational amplifier.

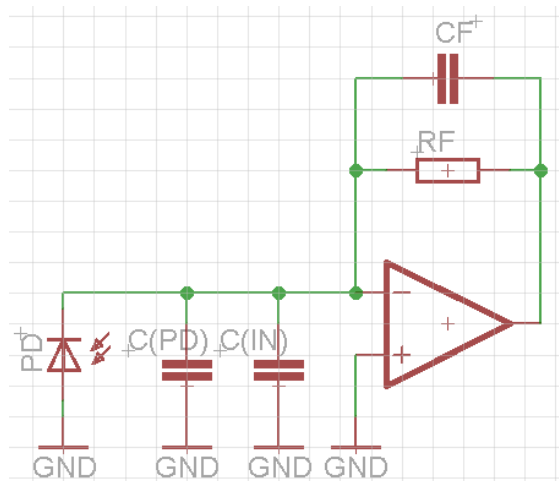


Figure 8. Transimpedance amplifier circuit.

The output voltage depending on the photodiodes current is shown in equation (10). As the op amp operates in inverting mode, the output voltage is negative. This equation only applies at low frequencies depending on the bandwidth of the system.

$$V_{out} = -I_{PD} * R_F \quad (10)$$

The main factors that affect the bandwidth of the system are the bandwidth of the op amp that is used, total input capacitance C_T that consists of photodiodes internal capacitance and op amps input capacitance, and the magnitude of feedback resistor.

Usually the photodiodes internal capacitance is much greater than the input capacitance of op amp, consequently the input capacitance of op amp can be neglected as it has very small effect on the bandwidth. Feedback capacitor C_F is introduced across R_F to compensate phase distortion that is caused by C_{PD} , as well as to maintain stability and minimize ringing. The following equations are used to theoretically calculate the value of feedback capacitor - equation (12) [14,49] and the expected -3dB bandwidth of the system - equation (11) [15,3]. In the equations GBW is gain-bandwidth product of the op amp. It is the product of open-loop voltage gain and the frequency at which the gain is measured.

$$f_{-3dB} = \sqrt{\frac{GBW}{2\pi C_T R_F}} \quad (11)$$

$$C_F = \sqrt{\frac{C_T}{2\pi R_F GBW}} \quad (12)$$

The value of feedback capacitor must be chosen carefully as overcompensating the system with a larger feedback capacitor will decrease the usable bandwidth, which is mainly a problem in high frequency applications. If the TIA is undercompensated then the ringing increases, as well as the system might become unstable and start oscillating [16].

The operational amplifier that is used in the TIA is LM348. It is a quad op amp consisting of four operational amplifiers in one package that have the characteristics of the novel 741 op amp. This op amp was chosen for the design because it is low cost and easily available as well the quad configuration is beneficial for a small size design. This op amp has a comparatively low GBW that is only 1 MHz, but, as will be shown in further calculations, the GBW is high enough for the intended application. Another characteristic that must be mentioned is the input capacitance of the op amp that is 1.4 pF. As previously mentioned the diode capacitance that in this case is 70 pF is much greater than the input capacitance of the op amp, accordingly the input capacitance of the op amp could be neglected. In the following calculations R_F is 1 MΩ whereas in the practical system it is a 1 MΩ trimmer permitting the adjustment of the amplification of the photodiodes current. By applying the equation (11) and (12) $f_{-3dB} = 47.2$ kHz and $C_F = 3.4$ pF. During prototyping and testing it was observed that the TIA operated more stably with higher feedback capacitor value, which could be explained with deviations in component values as well as parasitic components. In the design feedback capacitance is composed of a 10 pF

capacitor in parallel with a variable capacitor with capacitance of 2.8 pF to 12 pF. A variable capacitor is used so it would be possible to manually adjust it and compensate the TIA most precisely.

Another characteristic of op amp that introduces additional limitations is slew rate. Slew rate describes the maximum possible rate of change of the output voltage for an op amp circuit. If the slew rate is exceeded, the output voltage will be distorted. In equation (13) the slew rate condition is specified where f is the frequency of the output signal and V_{pk} is the peak voltage of the output signal.

$$\begin{aligned} SR &\geq 2\pi f V_{pk} \\ V_{pk} &\leq \frac{SR}{2\pi f} \\ f &\leq \frac{SR}{2\pi V_{pk}} \end{aligned} \quad (13)$$

As shown in the equation above to avoid exceeding the slew rate, either the frequency or the peak voltage of the output must be decreased. Slew rate of LM348 op amp is 0.5 V/ μ s. As will be shown in the following section of measurements the output peak voltage of the TIA at times rose up to 5 V. By knowing the maximum output peak voltage the maximum distortion free frequency can be calculated by equation (13) and it is approximately 16 kHz. Comparing it to the -3dB bandwidth of the TIA that is 47 kHz it can be seen that it is much lower. Therefore, to restore the bandwidth of the system the maximum output peak voltage should be reduced to 1.7 V.

3.2.2 Measurements

The measurement setup consists of the laser diode that is connected to a function generator "HAMEG HM 8030-5". The laser beam is modulated by the function generator to simulate real situation where the laser beam would be modulated by the vibration of the measured object. The laser beam is directed on the photodiode that is connected to the TIA. The output voltage of the TIA is measured with "HAMEG HM407" oscilloscope. Appendix 2 shows an image of the measurement setup. The TIA circuit is as shown in figure 8. Of course the C_{PD} and C_{IN} are internal capacitances. The value of R_F is 1 M Ω and C_F is adjusted in the range from 10 pF to 13 pF.

To calculate -3 dB voltage by knowing passband peak to peak voltage the equation (14) was used. In the equation V_{pp1} is the passband peak to peak voltage and V_{pp2} is the peak to peak voltage at -3 dB.

$$\begin{aligned}-3(dB) &= 20\lg\left(\frac{V_{pp2}}{V_{pp1}}\right) \\ V_{pp2} &= 10^{\frac{-3}{20}} * V_{pp1}\end{aligned}\quad (14)$$

V_{pp1} was measured with oscilloscope to be 2.5 V substituting this value in equation (14) the value of V_{pp2} was found to be 1.8 V. Afterwards by changing the laser frequency the point where voltage is 1.8 V was found and the corresponding -3 dB frequency was found to be approximately 13 kHz.

3.2.3 Simulation

In this chapter the simulation and measurement results will be presented and compared. The simulations presented in this and the following chapters were done using “Multisim 12.0” simulation software. The simulated TIA circuit is shown in figure 9.

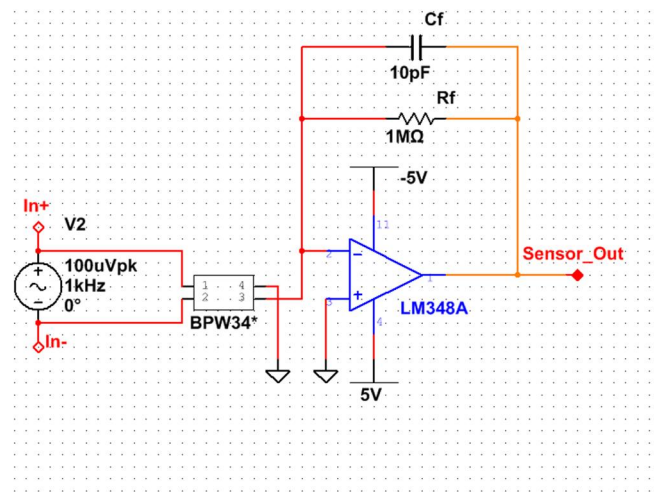


Figure 9. TIA simulation circuit with photodiode.

The model of the photodiode [17] simulates the operation of the BPW 34. Pin 1 is the positive optical input, pin 2 is negative optical input, pin 3 is cathode, and pin 4 is anode. A voltage source must be connected between optical input pins. As defined by the model 1mV voltage corresponds to light irradiance of 1 mW/cm². In the model of the photodiode the relative spectral sensitivity at certain wavelength must be specified. As the used laser has wavelength of 650 nm the relative spectral intensity is 0.6. Another thing that must be adjusted is the diode capacitance depicted as C_{j0} to be 70 pF.

The frequency response of the simulated circuit is shown in appendix 3. In the graph the green trace represents the frequency response when $C_F = 10\text{pF}$ and the red trace when

$C_F = 13\text{pF}$. The amplitude of the output is around 89.5 dB in the passband region, thus the -3 dB point is when the amplitude is 86.5 dB. The -3 dB frequency for the TIA circuit with 13 pF feedback capacitor is approximately 13 kHz and for 10 pF feedback capacitor it is approximately 17 kHz.

Comparing the measured -3dB frequency with the simulated one it can be seen that the simulation with 10pF feedback capacitor delivers frequency that is for 4 kHz higher than the measured value. If the feedback capacitor in simulation is changed to 13 pF the simulated and measured -3dB frequencies are the same. This could be explained with the fact that physically all components have parasitic impedance which then affect the practical measurements and of course the components have some tolerance level producing an additional error.

3.3 Filter Design

During the experimental part it was noticed that the artificial lighting of the room produces profoundly high interference and usually, depending on the positioning of the photodiode, exceeded the amplitude of the laser beam. The interfering frequency range from the lighting was around 50 Hz to 500 Hz. A high-pass filter with the corner frequency of 500 Hz was designed. Another filter, a low-pass filter, was designed to filter out the high frequency interference. The corner frequency of this filter was chosen to be 50 kHz as the maximum possible operational frequency of the system is 47 kHz as calculated by equation (11).

3.3.1 Theory and Design

It was decided to use an active filter as one of the proposed design requirements is to keep the size of the system to a minimum. Comparing higher order active filters to passive filters, active filters necessitate less space as well the size of inductors in passive filters at low frequencies are of a substantial size. Both of the filters are 4th order, Sallen-Key topology, Bessel type active filters. Sallen-Key topology was used mainly because of its simplicity. Bessel type was chosen because it produces maximally linear phase response, thus the distortion of the signal in the passband is very low. A 4th order filter is used because a steep cut-off slope is necessary and for 4th order filter it is 80 dB/decade.

LM348 op amp was used to design the active filters. As the package facilitates 4 op amps both of the 4th order filters were designed around one LM348 chip.

In figure 10 a schematic of the low pass filter can be seen. The values of the components are specified and the calculations will be shown in the following section. As can be seen in figure 10 the filters are operating at unity gain as no gain was necessary. Reducing the filter from general form to unity gain form the number of passive components needed for each stage was reduced by two, thus saving 8 passive components

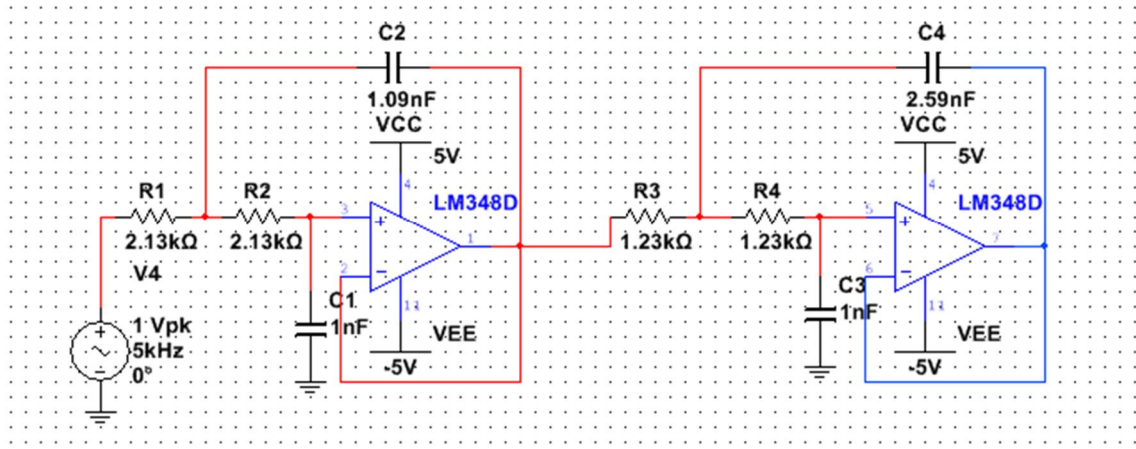


Figure 10. Schematic diagram of a 4th order low-pass filter with corner frequency 50 kHz.

In the coming equation the formulas and calculations of the necessary component values will be shown. The component names in the figure 10 correspond to the ones presented in equation (15) [18,20]. In the following equations f_c denotes corner frequency and a_n , b_n are filter coefficients for different order filters [18,56].

$$C_1 = C_3 = 1 \text{ nF}, a_1 = 1.3397, b_1 = 0.4889, a_2 = 0.7743, b_2 = 0.3890$$

$$C_2 \geq C_1 \frac{4b_1}{a_1^2} \geq 1.09 \text{ nF} \sim 1.1 \text{ nF}$$

$$C_4 \geq C_3 \frac{4b_2}{a_2^2} \geq 2.59 \text{ nF} \sim 2.7 \text{ nF}$$

$$R_{1,2} = \frac{a_1 C_2 \pm \sqrt{a_1^2 C_2^2 - 4b_1 C_1 C_2}}{4\pi f_{c1} C_1 C_2} = 2.13 \text{ k}\Omega \sim 2.2 \text{ k}\Omega$$

$$R_{3,4} = \frac{a_2 C_4 \pm \sqrt{a_2^2 C_4^2 - 4b_2 C_3 C_4}}{4\pi f_{c1} C_3 C_4} = 1.23 \text{ k}\Omega \sim 1.2 \text{ k}\Omega \quad (15)$$

The value for C_1 and C_3 was randomly chosen, though the nF magnitude was chosen to have the resistor values in the kΩ range. The component values are approximated to the closest value of the available components.

The high-pass filter was designed in a similar manner as the previous filter. Of course, the schematic diagram is different as shown in figure 11.

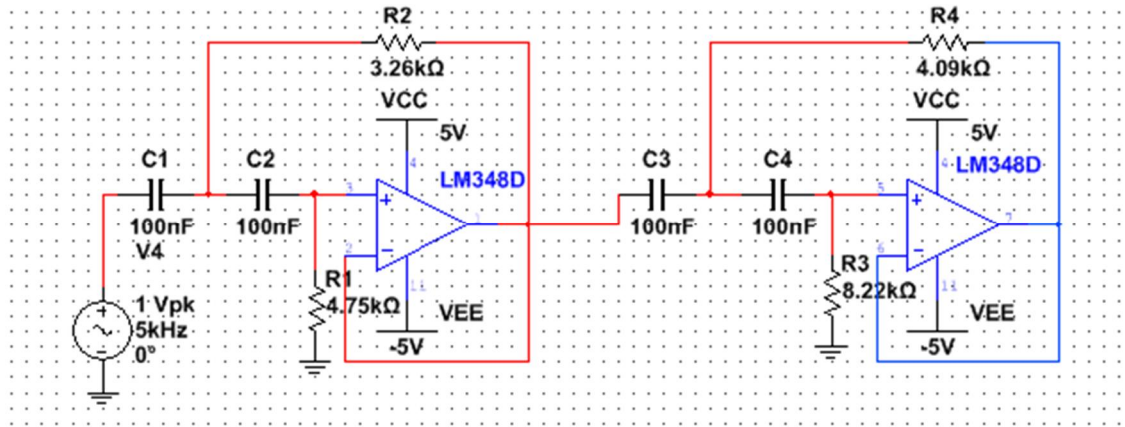


Figure 11. Schematic diagram of a 4th order high-pass filter with corner frequency 500 Hz.

The values for capacitors C_1 , C_2 , C_3 , C_4 were chosen so the resistor values would be in the low range of $k\Omega$ as it was done previously. In the following equation (16) [18,27] the calculations of the component values are shown.

$$\begin{aligned}
 C_1 = C_2 = C_3 = C_4 &= 100 \text{ nF}, a_1 = 1.3397, b_1 = 0.4889, a_2 = 0.7743, b_2 = 0.3890 \\
 R_1 &= \frac{1}{\pi f_{c2} C_1 a_1} = 4.75 \text{ k}\Omega \sim 4.7 \text{ k}\Omega \\
 R_2 &= \frac{1}{4\pi f_{c2} C_1 b_1} = 3.26 \text{ k}\Omega \sim 3.3 \text{ k}\Omega \\
 R_3 &= \frac{1}{\pi f_{c2} C_1 a_2} = 8.22 \text{ k}\Omega \sim 8.2 \text{ k}\Omega \\
 R_4 &= \frac{1}{4\pi f_{c2} C_1 b_2} = 4.09 \text{ k}\Omega \sim 3.9 \text{ k}\Omega
 \end{aligned} \tag{16}$$

The component calculated values are yet again approximated to the closest value of the available components.

The high-pass filter not only filters out the interfering signals from lighting but as well the possible vibration frequency. Therefore a switch is introduced in the design to either turn on the high-pass filter or to turn it off. For example, if it is known that the vibrational frequency of the object is in the range of 0 to 500 Hz the high-pass filter can be deactivated and only the low-pass filter will be connected in the circuit. In this kind of situation the artificial lighting should be minimized and it must be noted that if any artificial light is falling on the sensor it will disrupt the measurement.

3.3.2 Measurements and Simulation

The filter circuits were practically tested using the same tools as previously shown in TIA testing. Equation (14) was used to calculate the voltage amplitude that corresponds to the voltage at corner frequency. Measuring the high-pass filter the -3 dB corner frequency was found to be approximately 54.5 kHz and for the low-pass filter it was found to be approximately 700 Hz. The deviation from the theoretically calculated values can be explained with the component tolerances, parasitic components as well as the measurement error introduced by the precision of the oscilloscope.

In appendix 4 and appendix 5 the frequency responses of the low-pass and high-pass filter with theoretical values and approximated factual values can be seen. The red curve depicts the frequency response of the filter with factual values while the green curve is the theoretical frequency response. As can be seen the approximation of the component values caused very small change and both curves almost completely overlay.

3.4 Level Shifter

Level shifting in this system is necessary to condition the filtered output voltage of TIA for further signal analysis. The signal will be analysed by either a microcontroller or a computer. If a computer will be used the analog signal will be converted to a digital one using “NI myDAQ”. The analog to digital converter (ADC) of “NI myDAQ” can handle voltage levels up to ± 10 V [19,1], therefore if this device will be used no signal conditioning will be necessary. If a microcontroller will be used then it might be “Mbed” microcontroller. The ADC input voltage range of “Mbed” microcontroller is 0 to 3.3 V [20,101]. Usually the ADC input voltage of a microcontroller is positive, either it is in the range of 0 to 3.3 V or 0 to 5 V, thus a level shifter is necessary. The design of a level shifter which converts ± 5 V to 0 - 3.3 V range is discussed in this section.

3.4.1 Theory and Design

To convert ± 5 V voltage to 0 V - 3.3 V range two manipulations must be performed. Firstly the voltage must be attenuated to ± 1.65 V range and secondly a DC offset of 1.65 V must be added to the signal to rise it above negative voltage. Both of these actions will

be done using a non-inverting differential op amp circuit. The same operational amplifier LM348 will be used to design a level shifter.

In the following figure 12 a circuit diagram of the non-inverting differential amplifier, further in text referred to as level shifter, is presented.

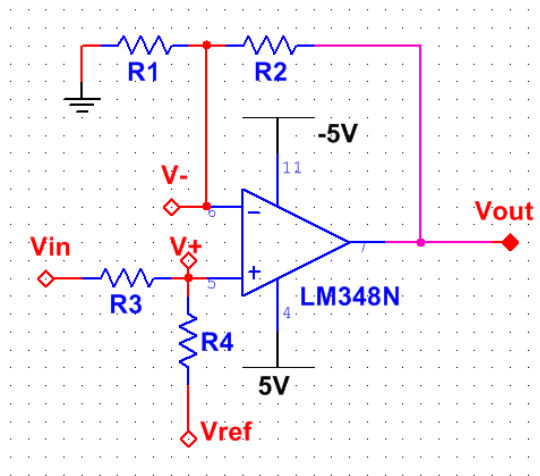


Figure 12. Schematic diagram of the level shifter circuit.

In figure 12 V_- is the voltage at the inverting input, V_+ is the voltage at the non-inverting input, V_{IN} is the input voltage, V_{REF} is the reference voltage, and V_{OUT} is the output voltage. In the equation (17), where A is the attenuation factor, circuit analysis of the level shifter will be done using nodal method.

$$\begin{cases} I_+ = \frac{V_{IN}-V_+}{R_3} \\ I_+ = \frac{V_+-V_{REF}}{R_4} \end{cases} \rightarrow \frac{V_{IN}-V_+}{R_3} = \frac{V_+-V_{REF}}{R_4} \rightarrow V_+ = \frac{V_{IN}R_4 + V_{REF}R_3}{R_3 + R_4}$$

$$\begin{cases} I_- = \frac{V_-}{R_1} \\ I_- = \frac{V_{OUT}-V_-}{R_2} \end{cases} \rightarrow \frac{V_-}{R_1} = \frac{V_{OUT}-V_-}{R_2} \rightarrow V_- = \frac{V_{OUT}R_1}{R_1 + R_2}$$

$$V_- = V_+ \rightarrow \frac{V_{OUT}R_1}{R_1 + R_2} = \frac{V_{IN}R_4 + V_{REF}R_3}{R_3 + R_4}$$

$$\text{If } V_{IN} = 0 \rightarrow \frac{V_{OUT}R_1}{R_1 + R_2} = \frac{V_{REF}R_3}{R_3 + R_4} \rightarrow V_{OUT} = V_{REF} \frac{R_3(R_1 + R_2)}{R_1(R_3 + R_4)}$$

$$\text{If } \begin{cases} R_1 = R_3 \\ R_2 = R_4 \end{cases} \rightarrow V_{OUT} = V_{REF} \frac{R_3}{R_1}$$

$$\text{If } V_{REF} = 0 \rightarrow \frac{V_{OUT}R_1}{R_1 + R_2} = \frac{V_{IN}R_4}{R_3 + R_4} \rightarrow V_{OUT} = V_{IN} \frac{R_4(R_1 + R_2)}{R_1(R_3 + R_4)}$$

$$\text{If } \begin{cases} R_1 = R_3 \\ R_2 = R_4 \end{cases} \rightarrow V_{OUT} = V_{IN} \frac{R_4}{R_1}$$

$$A = \frac{V_{OUT}}{V_{IN}} = \frac{R_4}{R_1} \quad (17)$$

The voltage attenuation must be 0.33 as the ± 5 V voltage must be decreased to ± 1.65 V and to avoid the voltage going negative a 1.65 V offset must be added to the ± 1.65 V voltage. Using the formulas that were derived in equation (17) it can be shown that if R_1 and R_3 is $100\text{ k}\Omega$ then R_2 and R_4 accordingly are $33\text{ k}\Omega$.

The necessary DC offset of 1.65 V was produced by a voltage divider as shown in figure 12.

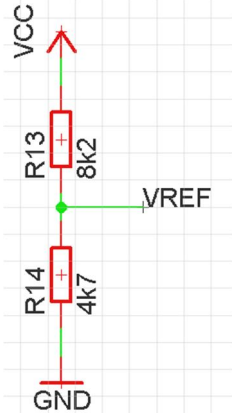


Figure 13. Voltage divider for reference voltage.

In figure 13 V_{CC} is the supply voltage and it is 4.5 V. Equation (18) shows the calculation of the resistor values. The circuit essentially is a simple voltage divider and the reference voltage V_{REF} is the voltage across resistor R_{14} .

$$V_{REF} = \frac{R_{14}}{R_{13} + R_{14}} V_{CC} \rightarrow R_{14} = \frac{V_{REF}}{V_{CC} - V_{REF}} R_{13} \quad (18)$$

If R_{13} is chosen to be $8.2\text{ k}\Omega$ then R_{14} should be $4.75\text{ k}\Omega$. The closest standard resistor value for R_{14} is $4.7\text{ k}\Omega$. Using previously derived values reference voltage is 1.64 V which is acceptable. The voltage divider is connected to the level shifter at R_4 as shown in figure 12. Resistor values in the voltage divider must be as low as possible to not to disturb the level shifter, but they must be as well high enough so the current through the resistor would be kept to minimum. As the resistor values in the level shifter are in the magnitude of tens of $\text{k}\Omega$ the resistor values for voltage divider were chosen to be in the $\text{k}\Omega$ range.

3.4.2 Simulation and Measurements

The simulation of the level shifter was carried out. The amplitudes of input and output voltages are shown in appendix 6. The input voltage is 10 V_{PP} and, as can be seen from

appendix 6, the output voltage is approximately $3.3 \text{ V}_{\text{PP}}$ and the offset voltage is correct as the output voltage does not go negative.

By measuring the constructed level shifter circuit the DC offset voltage was found to be approximately 1.6 V which is for 0.05 V lower than the theoretical values. As well, the voltage attenuation was found to be 0.37 not 0.33. The deviations from the theoretically calculated values can be explained with components tolerances, parasitic components, and another cause of error would be previously mentioned effect caused by the reference voltage divider.

3.5 Voltage Rail Splitter

It was planned to use a PP3 nine-volt battery for the circuit voltage supply as it is easily accessible and the capacity is high enough to power the system for a sufficient time. As LM348 op amp necessitates a dual voltage supply several ways of supply were considered. The easiest and most straight forward solution would be to use two voltage sources for positive and negative voltage. While this kind of solution is easily achievable with a power supply, which has at least two voltage sources, it is not so simple to do it with batteries. For example, if two batteries are used to create a positive and negative supply the main problem would be the instability of voltages. The instability is caused by the different voltage levels of each battery and if the batteries are not discharged evenly then the voltage difference will become even bigger. Because operational amplifiers require a constant and balanced voltage supply the use of two batteries is not sufficient.

Another simple way would be to use a voltage divider with two equal resistors which would divide the voltage and create a virtual ground at the midpoint. In this case, if the resistor impedance would be big comparing to the circuit that must be supplied, the supply voltage would be divided between the load and one of the supply resistors. Additionally, if positive and negative poles would be loaded unsymmetrically, the voltage supply would become unbalanced and a voltage difference would arise between positive and negative pole. In the case where the resistor impedance would be low, even though the previously mentioned problem would be solved, another problem would arise. Since decreasing the resistor impedance the standby current through the resistors would increase and the battery life would be unnecessarily decreased.

To resolve the previously mentioned problems an op amp circuit, which will be described in more detail later, can be used as a voltage rail splitter. This circuit provides a stable division of the single supply voltage and produces reliable virtual ground. The standby power consumption of the circuit is comparatively small and the output impedance of the system as it is for op amps is very low.

The circuit diagram of the rail splitter is shown in figure 14 and the operational principle is described below.

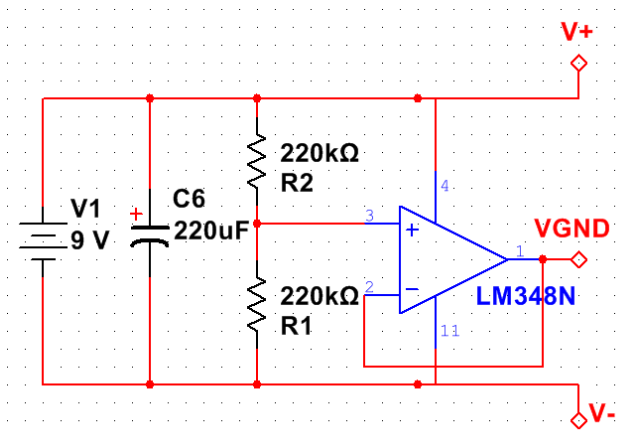


Figure 14. Voltage rail splitter circuit diagram.

The battery voltage is divided in half with the $220\text{ k}\Omega$ voltage divider and the midpoint is connected to the non-inverting input of the op amp. The inverting input is connected straight to output, thus transforming this circuit into a voltage follower. The voltage at the non-inverting input is 4.5 V and the same voltage appears at the output of the op amp. Now the output of the op amp is the virtual ground, positive voltage supply is 4.5 V and negative voltage supply is -4.5 V. A bypass capacitor is introduced across the battery to filter out any AC fluctuations that may arise. Despite all the positive aspects of this circuit there is one drawback of this circuit. The maximum output current depends on the maximum output current of the op amp that usually is in the range of tens of milliamps. In the design LM348 op amp is used and its output short circuit current is 25 mA, thus the maximum permissible output current cannot exceed 25 mA.

The circuit was constructed and tested. It was discovered that the positive voltage was by 0.01 V higher than the negative voltage. The reason for this difference is the tolerance of the resistors used to split the voltage. As the difference is very low more precise resistors were not sought.

3.6 Component Selection

In this chapter the component selection is described. All in all 29 passive components, of which 17 are resistors and 12 are capacitors, and 2 op amp chips are used. Altogether 7 op amps are necessary - four for the two filters, one for TIA, one for level shifter, and one for voltage rail splitter. One of the requirements for the system is to be of small size, thus the LM348 op amp was chosen. It accommodates four op amps in one 14 pin chip. It is available in SOIC 14 package which has the dimensions of 6 x 8.6 mm. One LM348 chip is designated particularly for the two filters and the second chip will be used with the other three circuits hence leaving one op amp unused. The supply current of each op amp maximally is 0.6 mA altogether for both op amp chips adding up to 5.6 mA. [21]

Almost all of the passive components are in surface-mount device (SMD) 3216 package. The size of the 3216 package components is 3.2 x 1.6 mm. The maximum power rating for this package is 0.25 W. In the circuit the highest possible power consumption can be through the 1.2 kΩ resistors in the filters. The calculation of the maximum possible power dissipation on these components is shown in equation (19) where V is voltage V_{rms} is the root mean square voltage of an AC voltage, and P is power.

$$\left\{ \begin{array}{l} V_{rms} = \frac{V_{pp}}{\sqrt{2}} \\ P = IV \\ I = \frac{V}{R} \end{array} \right. \rightarrow P = \frac{V_{rms}^2}{R} \quad (19)$$

The maximum peak to peak output voltage swing of TIA is 9 V as the supply is ±4.5 V. Substituting the voltage and resistance values in the equation (19) the maximum power dissipation is calculated to be 0.034 W. The smallest SMD package that could be used for the passive components is 0603 as the power rating for it is 0.05 W. The power rating of 1206 is more than sufficient and smaller components could have been used, but with smaller packages the soldering process would be much more challenging and time consuming.

There are three single inline package (SIP) connectors designated for the output voltage. One pin is the ground, second is unregulated voltage output and third pin is the regulated output voltage. Another four SIP connectors are used to connect the photodiode and the laser. As previously explained, there is a switch to turn the high-pass filter on or off. Lastly, a screw connector for battery connection is used.

3.7 Printed Circuit Board Design

A printed circuit board (PCB) was made of the whole system. The schematic and layout design was done with PCB design software “Eagle”. The PCB was milled using “LPKF ProtoMat S62” milling machine and a “LPKF ZelFlow R04” reflow oven was used to solder the SMD components. The through-hole components were soldered manually with a soldering iron. Two boards were created. On one board all of the analog signal processing circuits were placed, whereas the other board held the laser and photodiodes. Components on the main board were placed as compactly as possible. The 2 potentiometers, adjustable capacitor, switch and SIP connectors were placed on the side of the board to ease the access to those components. The two LM348 chips were placed in the middle of the PCB and the rest of the passive components were distributed around the chips. Complete schematic diagram and layout of the main board is shown in appendices 7 and 8 accordingly. The size of the main board is 38.7 mm x 46.0 mm. The final PCB with all of the components is shown in figure 15.

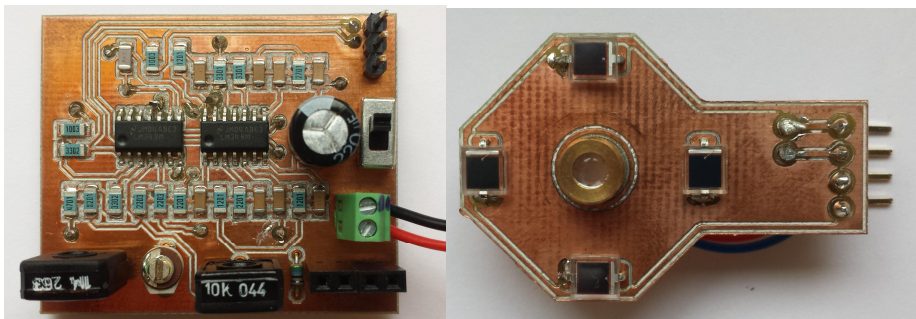


Figure 15. The final PCB and the laser-photodiode board.

The connection between the main board and laser-photodiode board was done with 4 SIP connectors shown in figure 15 in the lower right corner of the main PCB. The design of the laser-photodiode board was made to simplify the aiming process in short distances. The laser was placed in the middle while four photodiodes were placed around it thus the reflected beam can be detected by any of the four photodiodes. In the circuit the photodiodes were connected in parallel. The total capacitance created by the internal capacitances of the four photodiodes, as explained in chapter 3.2.1, must be compensated by the feedback capacitor and it can be done by adjusting the variable capacitor. Depending on the necessary measurement setup and distance the laser-photodiode board can be redesigned for a specific application. Also, if it is necessary, the laser and diode can be connected to the main board simply with wires so allowing to place the main board separately from the laser and photodiode.

4 Measurements Results and Suggestions

4.1 Measurement Results

All in all three kinds of measurements were conducted to determine the frequency bandwidth and operational characteristics of the developed GLV system. The first measurement setup can be seen in appendix 2. The laser is pointed directly on the photodiode. The laser diode is supplied by a DC voltage of around 2.5 V and an AC voltage of approximately 20 mV. This measurement setup simulates a situation where the main difference from a real life event is that the amplitude of change, which is created by the AC modulation of the laser beam, is constant over the measured frequency range. Using this measurement setup the frequency response of the system was determined. In figure 16 the measured frequency response is shown.

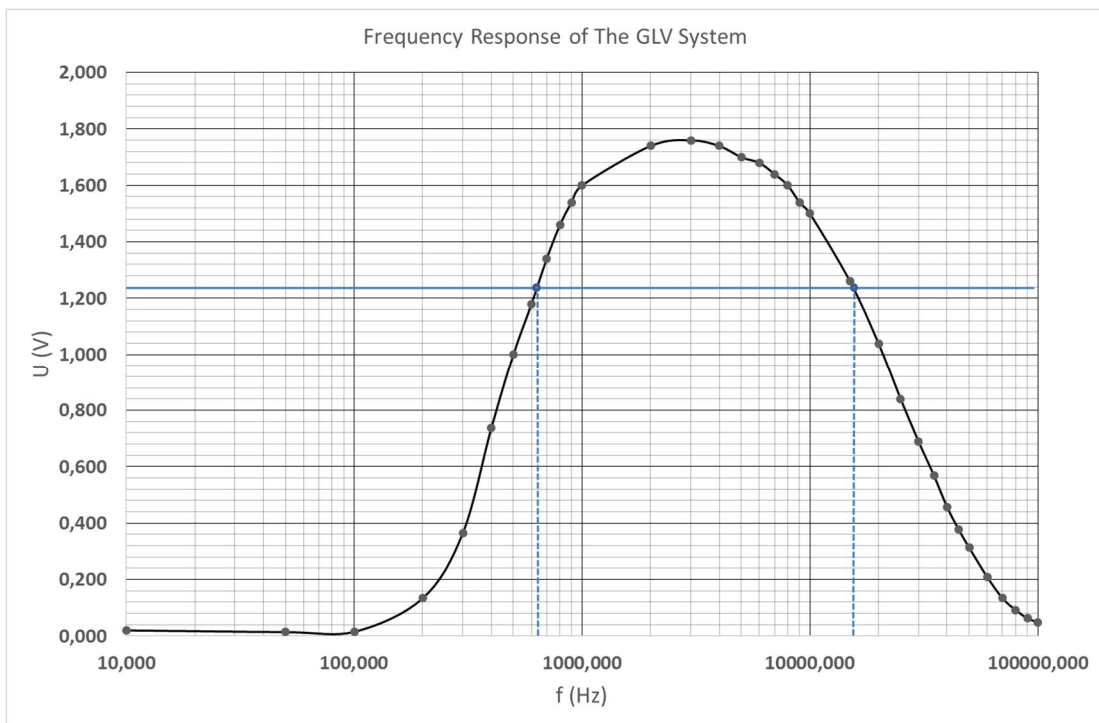


Figure 16. Frequency response of the GLV system.

The blue horizontal line marks the -3 dB voltage that was calculated using equation (14). The V_{PP1} in this case denotes the highest peak to peak voltage in the pass-band that is 1.76 V. By using this value it is determined that -3 dB voltage V_{PP2} is 1.24 V. The blue points mark the intersection with the frequency response line. These points mark the -3 dB frequency. The high-pass corner frequency is a bit over 600 Hz and low-pass corner

frequency is slightly over 15 kHz. Theoretically the high-pass corner frequency should correspond to the corner frequency of the high-pass filter that is approximately 700 Hz and the low-pass corner frequency should correspond to the corner frequency of the TIA that is in the range of 17 kHz depending on the value of the feedback capacitor. It can be seen that there is a modest deviation between the values. The main reason for this difference is that during measurement the position of the laser beam on the photodiode changed slightly and a small change in position of the laser beam caused noticeable change in the output voltage level of the TIA. Even though the laser beam was adjusted to a certain voltage at specific frequency several times during the measurement, still small error could arise because of the change in position. In appendix 9 the theoretical frequency response of the whole systems simulation is shown. As shown in appendix 9 the high-pass corner frequency is around 650 Hz and low-pass corner frequency is approximately 17 kHz, which corresponds to the previously shown values.

It was noticed that if the ambient light level was too high the output of the system became saturated, therefore the amplification level of the TIA had to be decreased with the potentiometer that is denoted as R16 in the layout of the schematic shown in appendix 8.

If the high-pass filter was turned off two things could be observed, firstly the output AC voltage started fluctuating and secondly a DC component appeared in the output voltage. The second point can be explained with the fact that there is a DC component in the output of the TIA and while the high-pass filter was in the circuit it was filtering it out. However, the first point can be explained with that the lighting of the room interfered with the laser beam and the interference diminished as the lighting was turned off.

The operation of the potentiometers and variable capacitor was tested as well. Adjustment of each of the component produced the expected results. If the TIA gain controlling potentiometer was adjusted the output voltage level changed, if the laser brightness potentiometer was adjusted the brightness of the laser changed, and if the variable feedback capacitor was adjusted a change in the output voltage could be observed. The filter switch, as explained previously, worked appropriately meaning that in one position both filters are operating while in the other position the high-pass filter was turned off keeping the low-pass filter on. The output OUT1 delivered unmodulated signal while the output OUT2 delivered expected level shifted output voltage.

The second measurement setup is different from the first one. In this case the laser beam was not directed straight onto the photodiode but onto a reflective surface. This surface is attached to a speaker hence simulating a real vibrating object. The speaker was driven by a function generator allowing the control of vibrational frequency. The reflected laser beam was directed onto the photodiode to detect the vibrational frequency. The distance between the speaker and the photodiode was approximately 1 m. The output voltage was not measured with an oscilloscope as previously but using "NI myDAQ". "NI myDAQ" is a data acquisition device produced by "National Instruments". The key specification points are as follows, the ADC resolution is 16 bits, maximum sampling rate is 200 kS/s, ± 10 V maximum analog input voltage, and the -3 dB passband of the analog input is DC to 400 kHz. As previously shown the high pass -3 dB frequency of the system is around 17 kHz with maximum output voltage of ± 5 V, thus it can be concluded that "NI myDAQ" is absolutely suitable device for the acquisition of the GLV systems output voltage.

The acquired signal was processed using "NI LabVIEW" which is a graphical programming software. In the program a digital low-pass filter with adjustable cut-off frequency was used to eliminate high frequency noise. The cut-off frequency was adjusted in the range of 5 kHz to 20 kHz depending on the measurement. To determine the detected vibrational frequency Fast Fourier Transform (FFT) is performed on the input signal and is represented in a graphical way, and the value of the frequency was determined using the "Tone Measurements Express VI" as shown in appendix 10.

The maximum detectable frequency was determined using the measurement setup where the reflective surface is attached to the speaker. In this setup the speaker was driven by a voltage with frequency in the range of 10 Hz to 20 kHz. The sound level was comparatively low but audible. Maximum detectable frequency was determined to be approximately 12 kHz. After the 12 kHz frequency it was not possible to distinguish the vibration frequency from the noise floor.

In the third measurement setup the reflecting surface was fixed on a stand with clamps and the speaker was positioned approximately 10 cm away from the reflecting surface. In this measurement with the same sound level as previously the maximum detectable frequency was determined to be below 5 kHz.

In figure 17 the graph window of FFT is shown. The horizontal axis shows the frequency in Hz while the vertical axis shows the amplitude of the frequency component.

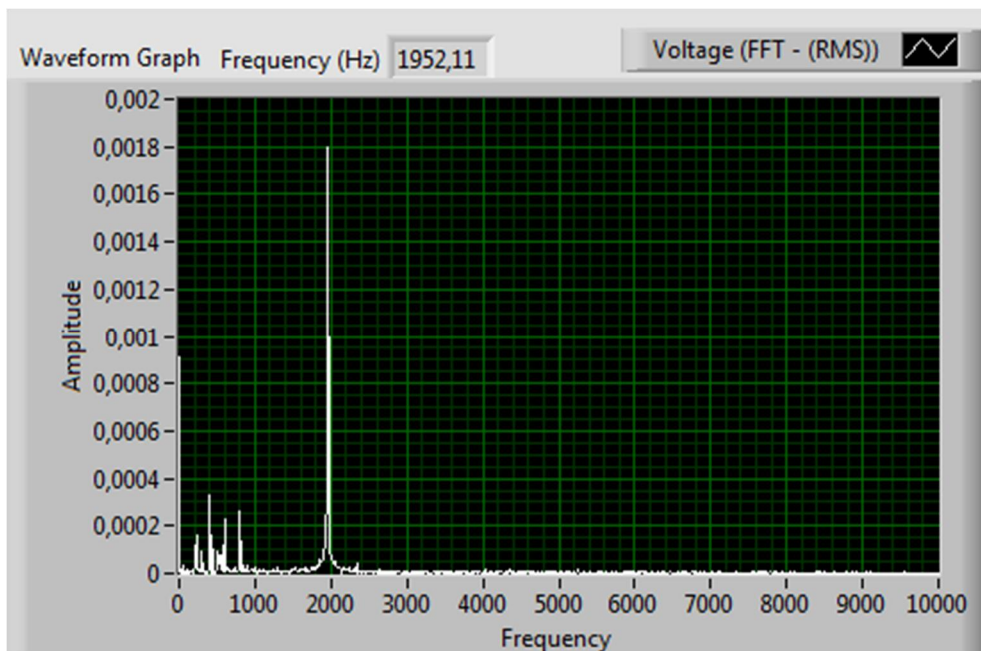


Figure 17. FFT of GLV systems output voltage.

In figure 17 the speaker was driven by a voltage with frequency of 1952 Hz and as can be seen it was easily detected. It was discovered that the frequency components visible in the frequency range below 1 kHz were generated by the oscilloscopes fan. As the oscilloscope was positioned on the same table with laser and photodiode the vibrations of the oscilloscopes fan were transmitted to the system through table.

The decrease in maximum detectable frequency from measurement setup two to three can be explained with the decreased intensity of the vibration of the vibrating surface. In measurement setup two the vibration was passed from the speaker on to the reflective surface straight away, while in measurement setup three the speaker introduced vibration in the air and that air vibration transferred the vibration to the reflective surface. Because of the energy lost during the transfer process the intensity of vibration is much lower in measurement setup three.

The operational current was measured to be 2.5 mA for the main board and 10 mA for the laser. If the consumed power is calculated by formula shown in equation 20 it is 22.5 mW for the main board and approximately 30 mW for the laser

$$P = IU \quad (20)$$

4.2 Flow Diagram of GLV System

In this chapter the operation of the system is summarized. The following figure 18 shows the operational processes in a simplified flow diagram showing all of the process steps and circuits contained in the main board and the laser-photodiode board.

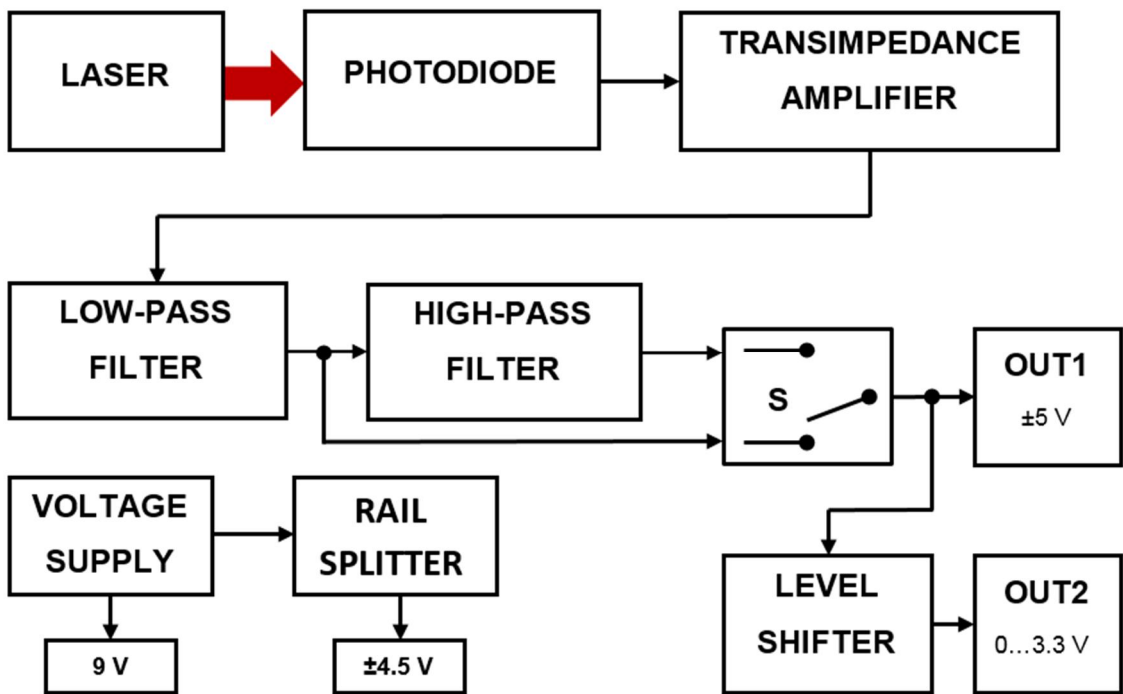


Figure 18. Flow diagram of the system.

The laser beam is directed onto a vibrating object where it is modulated depending on the intensity and frequency of vibration. The reflected beam is collected on a photodiode that is connected to a transimpedance amplifier. The modulated laser beam causes a varying current flow through the photodiode that is amplified and converted into voltage with TIA. The output voltage of the TIA is filtered using two filters - low-pass filter and high-pass filter. The low-pass filter has corner frequency of approximately 47 kHz, thus attenuating voltages above that set frequency and eliminating high frequency noise. While the high-pass filter has a corner frequency of approximately 700 Hz and its main function is to eliminate low frequency interference caused by artificial lighting.

The outputs of the filters are connected to a switch which can switch between the two outputs. If low frequency vibration measurements below 700 Hz must be carried out with the high-pass filter being in the circuit, it will attenuate not only the interference but the measured signal as well. Therefore the switch is introduced to obtain the possibility of

turning of the high-pass filter and measuring low frequency vibrations. However, it must be noted that without the high-pass filter the artificial lighting level must be kept to a minimum so the distortion of vibration signal would be as small as possible. At the output of the switch a filtered unregulated vibration signal voltage of maximum ± 4.5 V is present. This voltage afterwards is attenuated and shifted with level shifter, thus producing 0...3.3 V voltage that can be inputted in an analog to digital converter.

The circuit is supplied by a PP3 nine-volt battery. As the operational amplifiers necessitate a dual voltage supply a virtual ground is produced using the rail splitter circuit, thus creating ± 4.5 V. All of the circuits besides laser diode are supplied by the rail splitter. As the output current is limited to the maximum output current of the operational amplifier used in the rail splitter circuit that is 20 mA, the laser diode, because of its comparatively large current consumption, is supplied straight from the battery. The total power consumption of the whole system depending on the brightness of the laser maximally reaches 55 mW, thus providing comparatively long operating time.

5 Conclusion and Discussion

The thesis explains the operational principles of two kinds of laser vibrometers - laser Doppler vibrometer and grazing laser vibrometer. The commercially available systems employ the phenomena of Doppler Effect and interference, hence achieving great sensitivity and high detectable vibrational frequency range. But as with any high-end device the price of these systems is high as well. A low cost grazing laser vibrometer system was developed, thus fulfilling the aim of this thesis. Even though the sensitivity and detectable vibrational frequency range is not comparable to the commercially available devices, the system is fully functional and capable of detecting vibrational frequencies over 10 kHz frequency depending on the measurement setup and intensity of the measured vibrations.

Maximum detectable vibrational frequency measurements were conducted as described in thesis, but no sensitivity measurements were carried out. It is suggested that such a test would be carried out to determine the detectable frequency range depending on the intensity or amplitude of the vibration. This information would be beneficial in determining other possible applications of the developed GLV system.

There are few improvements that are suggested for increasing the quality of the system. First of all to increase the bandwidth and thus the maximum detectable frequency of the system, high speed operational amplifiers should be used in the design. Even though it would increase the total price of the system, it is considered that the benefits would be substantial as LM348 is comparatively slow operational amplifier with gain bandwidth product of only 1 MHZ. Another drawback of using a different operational amplifier is the possibility that it would not have a quad or even dual package so increasing the size of the main board. To decrease the interference from ambient lighting a photodiode with more narrow response to specific laser light should be used. The photodiode that is used in this system has maximum spectral intensity at wavelength of 900 nm while the relative spectral intensity to the used red laser light is only 60 %. Additionally optical filters can be introduced to filter out only the light produced by the laser. But, as previously mentioned, this improvement too would increase the size and cost of the system.

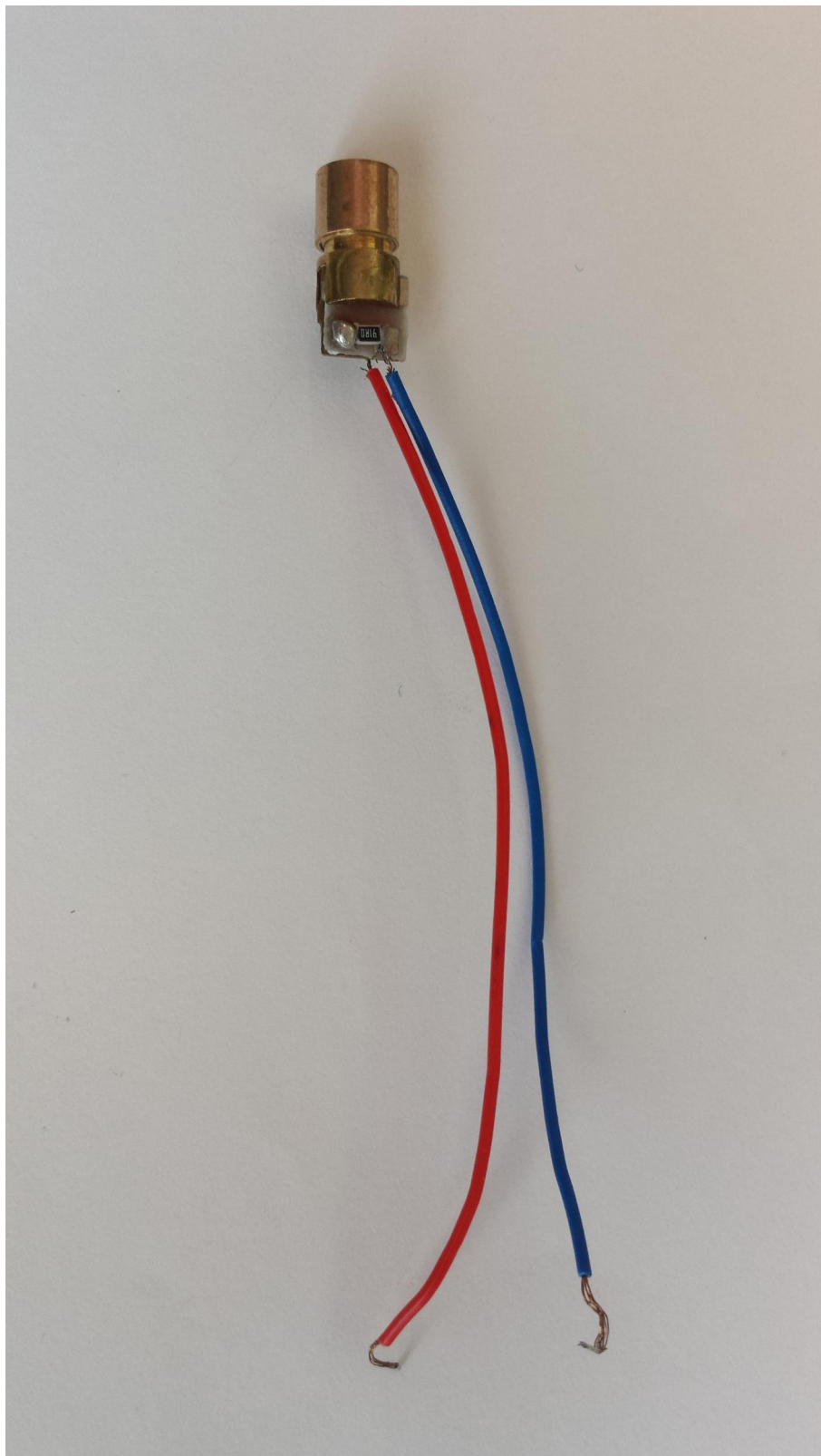
It can be concluded that overall the proposed aims were achieved and a low cost laser vibrometer system was developed. The costs of the system without the analysis or acquisition tools like “NI myDaq” or a signal processing microcontroller are below 5 euros, thus fulfilling the low cost condition. Even though the system has rather low sensitivity it is capable of detecting vibration of an object non-intrusively.

References

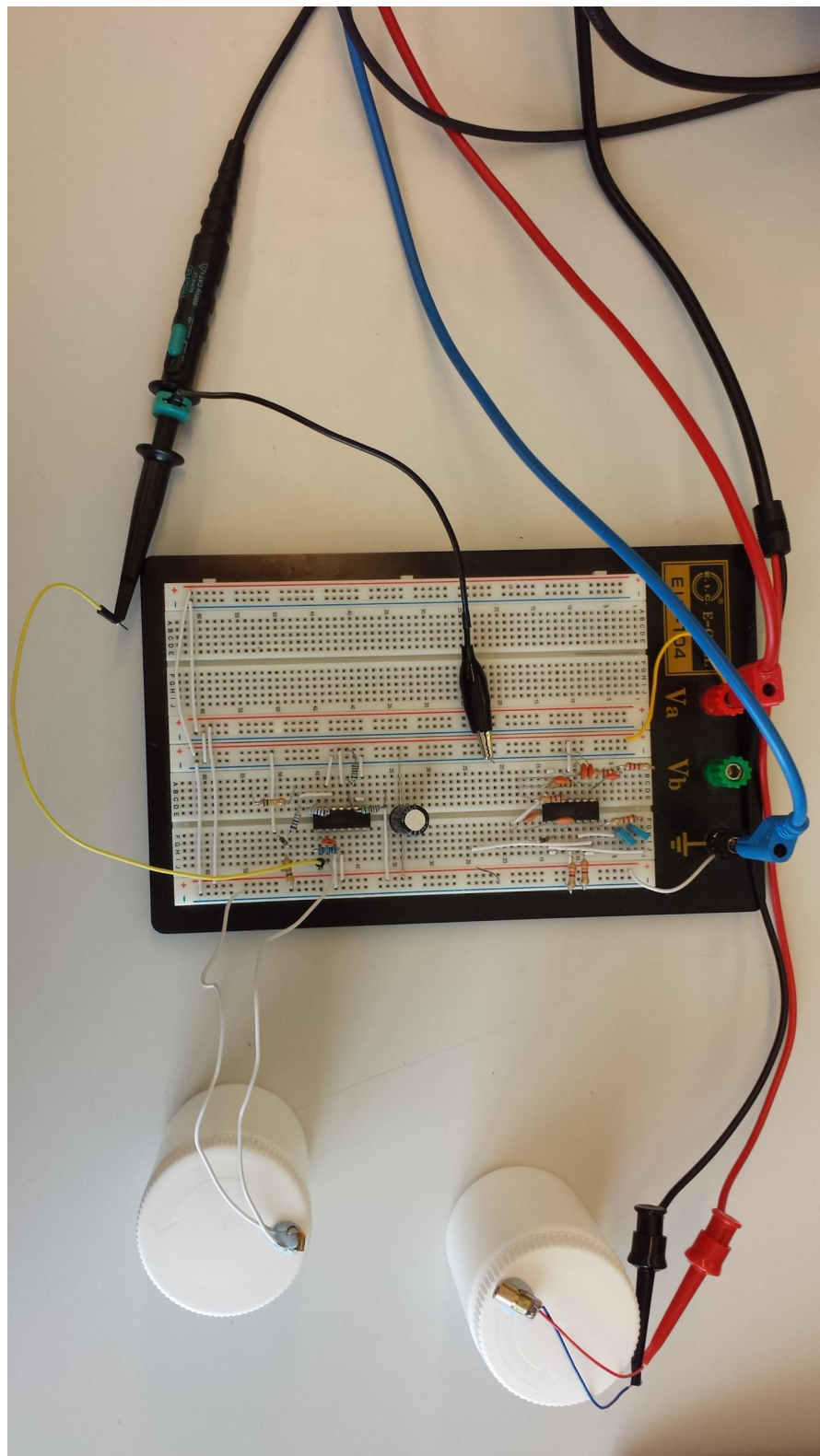
- 1 Bulat M. Galeev, "Light and Shadows of a Great Life: In Commemoration of the One-Hundredth Anniversary of the Birth of Leon Theremin, Pioneer of Electronic Art" 1999. [Online]. Available: <http://leonardo.info/isast/journal/journal96/LMJ6/galeyevintro.html>. [Accessed 17 March 2015].
- 2 "Polytec", "Laser Vibrometers and Velocimeters, Optical Measurement Solutions for Vibration, Length and Speed". [Online]. http://www.polytec.com/fileadmin/user_uploads/Products/Vibrometers/LM_Vibrometer_Flyer/Documents/OM_BR_ProductFlyer_2014_04_1000_E.pdf. [Accessed 25 March 2015].
- 3 "Argo-A Security", "Long-Range Laser Listening Device". [Online]. Available: http://argoasecurity.com/index.php?route=product/product&path=8&product_id=263. [Accessed 25 March 2015].
- 4 Al-Azzawi A. Physical Optics: Principles and Particles. 6000 Broken Sound Parkway NW, Suite 300: Taylor and Francis Group CRC Press; 2007
- 5 Shamir J. Optical Systems and Processes. P.O. Box 10, Bellingham, Washington 98227-0010: SPIE - The International Society for Optical Engineering; 1999
- 6 Shadrach C, Vadivelu S. Engineering Physics. India: Dorling Kindersley; 2010
- 7 Koechner W. Solid-State Laser Engineering.233 Spring Street, New York, NY 10013, USA: Springer Science + Business Media Inc.; 2006
- 8 Chen VC. The Micro-Doppler Effect in Radar. 685 Canton Street, Norwood, MA 02062: ARTECH HOUSE; 2011
- 9 "Polytec", "Measurement Solutions Made Possible by Laser Vibrometry". [Online]. http://www.polytec.com/fileadmin/user_uploads/Applications/Polytec_Tutorial/Documents/LM_AN_INFO_0103_E_Tutorial_Vibrometry.pdf. [Accessed 25 March 2015].
- 10 "Polytec", "UHF-120 Ultra High Frequency Vibrometer". [Online]. http://www.polytec.com/fileadmin/user_uploads/Products/Vibrometers/UHF-120/Documents/OM_DS_UHF-120_2014_10_PDF_E.pdf. [Accessed 25 March 2015].
- 11 Henderson R, Schulmeister K. Laser Safety. 270 Madison Avenue, New York, NY 10016: Taylor and Francis Group; 2004
- 12 Yoshizawa T, editor. Handbook of Optical Metrology, Principles and Applications, 6000 Broken Sound Parkway NW, Suite 300: Taylor and Francis Group CRC Press; 2009
- 13 "Vishay", "BPW34, Silicon PIN photodiode Datasheet". [Online]. <http://www.vishay.com/docs/81521/bpw34.pdf>. [Accessed 25 March 2015].
- 14 Graeme J. Photodiode Amplifiers, Op Amp Solutions. USA: McGraw-Hill Companies, Inc.; 1996

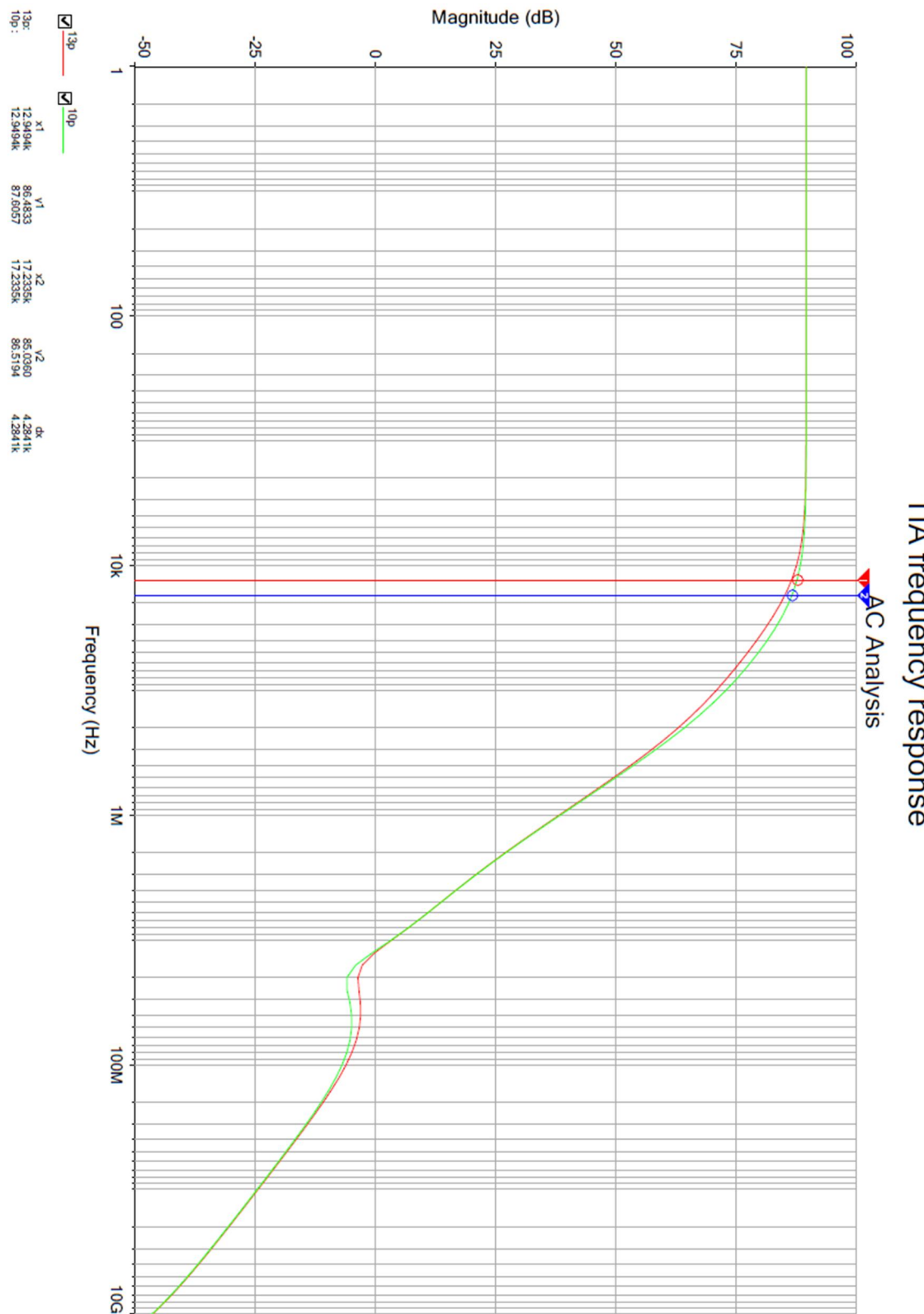
- 15 "Texas Instruments", "AN-1803 Design Considerations for a Transimpedance Amplifier". [Online]. <http://www.ti.com/lit/an/snoa515a/snoa515a.pdf>. [Accessed 25 March 2015].
- 16 Akshay Bhat, "Application Note 5129, Stabilize Your Transimpedance Amplifier". [Online]. <http://pdfserv.maximintegrated.com/en/an/TUT5129.pdf>. [Accessed 25 March 2015].
- 17 "OSRAM OS", "PSPICE Library for Photodiodes". [Online]. <http://www.osram-os.com/downloads/os-files/Electrical%20Simulation/IR/Silicon%20Photodetectors/PSpice%20Libraries/OSRAM%20Photodiodes%20II.lib>. [Accessed 25 March 2015].
- 18 "Texas Instruments", "SLOA088 Active Filter Design Techniques". [Online]. <http://www.ti.com/lit/ml/sloa088/sloa088.pdf>. [Accessed 25 March 2015].
- 19 "National Instruments", "Specifications NI myDAQ". [Online]. <http://www.ni.com/pdf/manuals/373061f.pdf>. [Accessed 25 March 2015].
- 20 "NXP", "UM10360 LPC173x/5x User Manual". [Online]. http://www.nxp.com/documents/user_manual/UM10360.pdf. [Accessed 25 March 2015].
- 21 "Texas Instruments", "LM148/LM248/LM348 Quad 741 Op Amps Datasheet". [Online]. <http://www.ti.com/lit/ds/symlink/lm148-n.pdf>. [Accessed 25 March 2015].

Laser

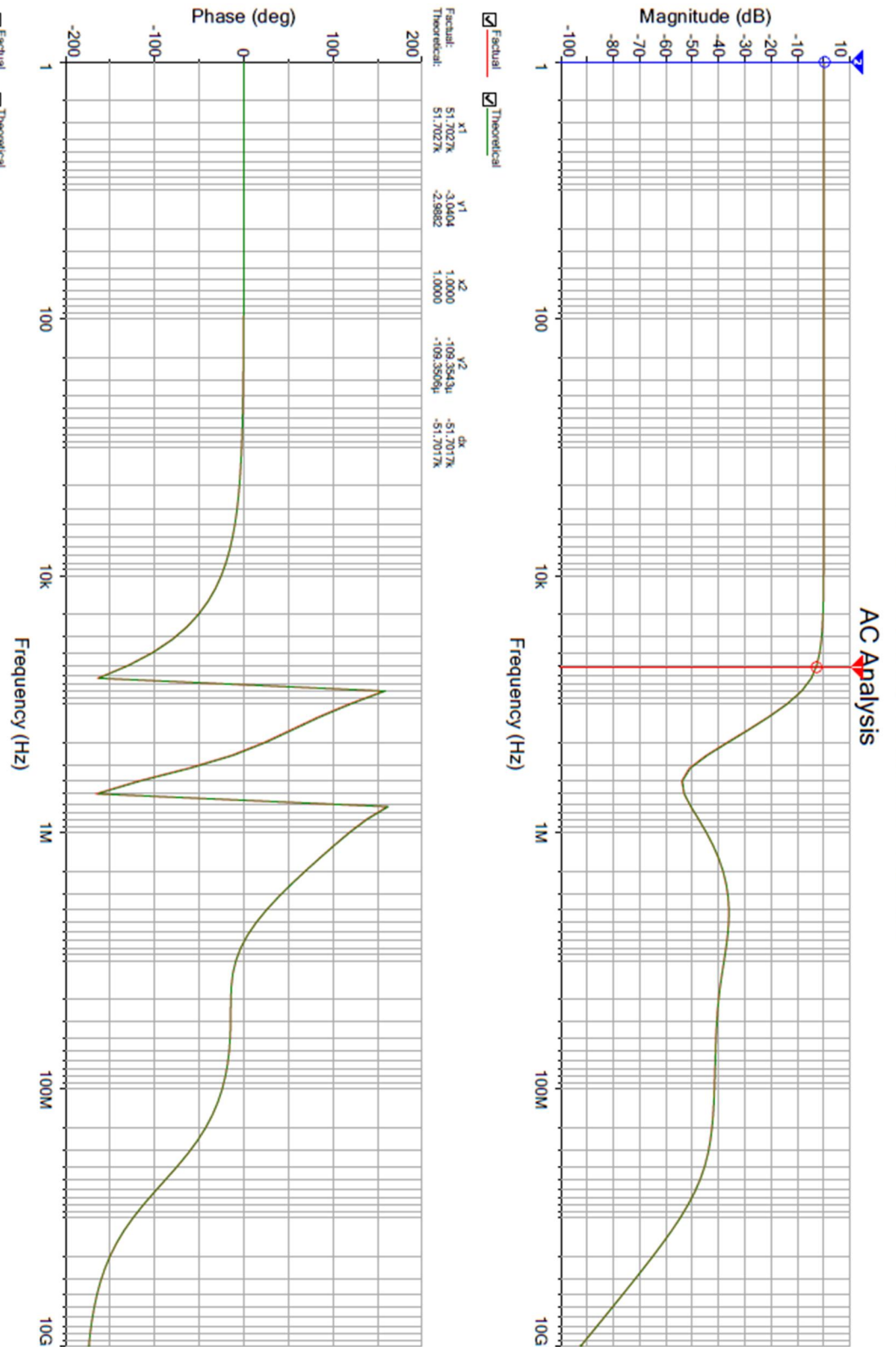


Measurement Setup



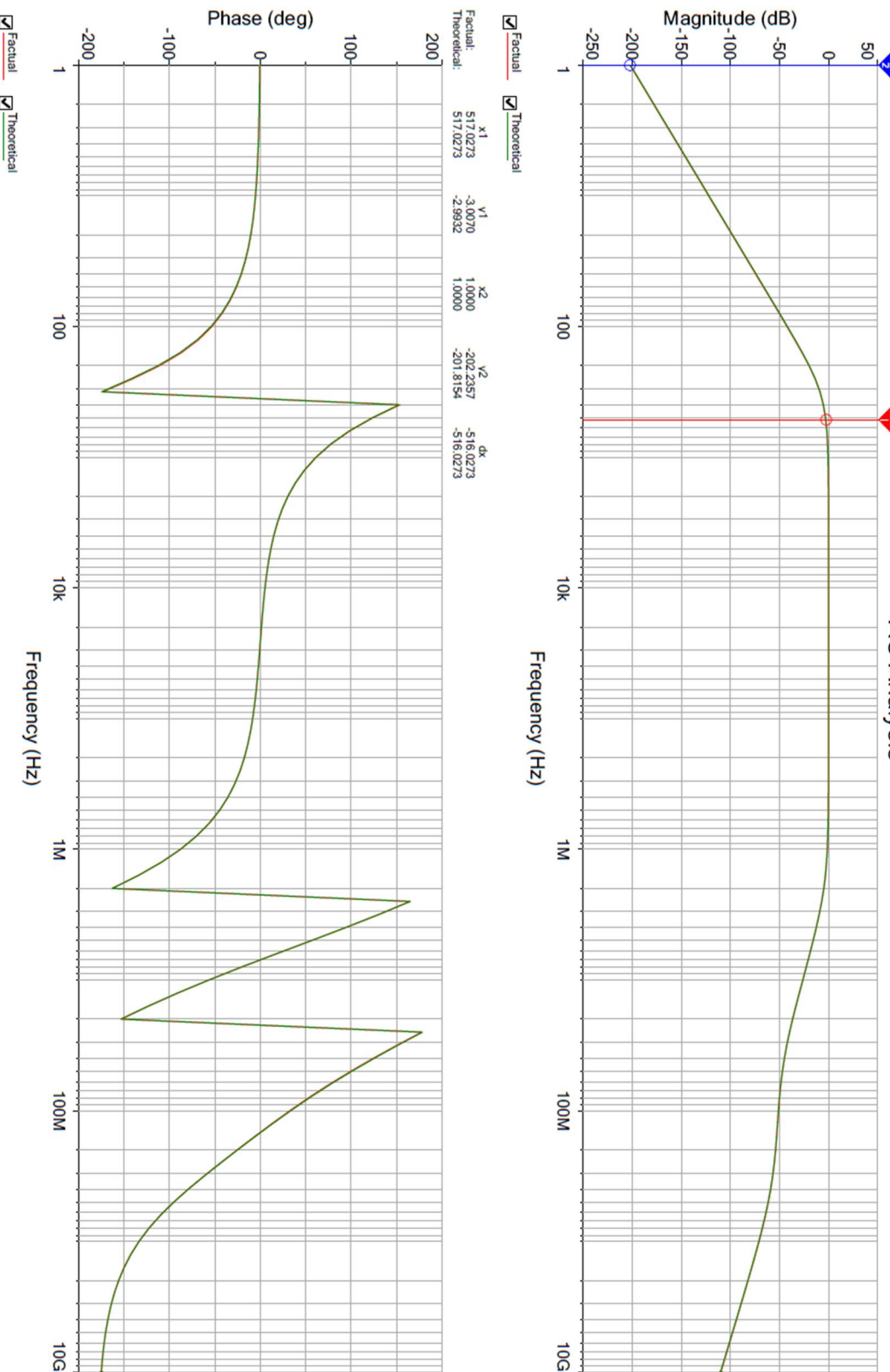
Frequency response of TIA simulation

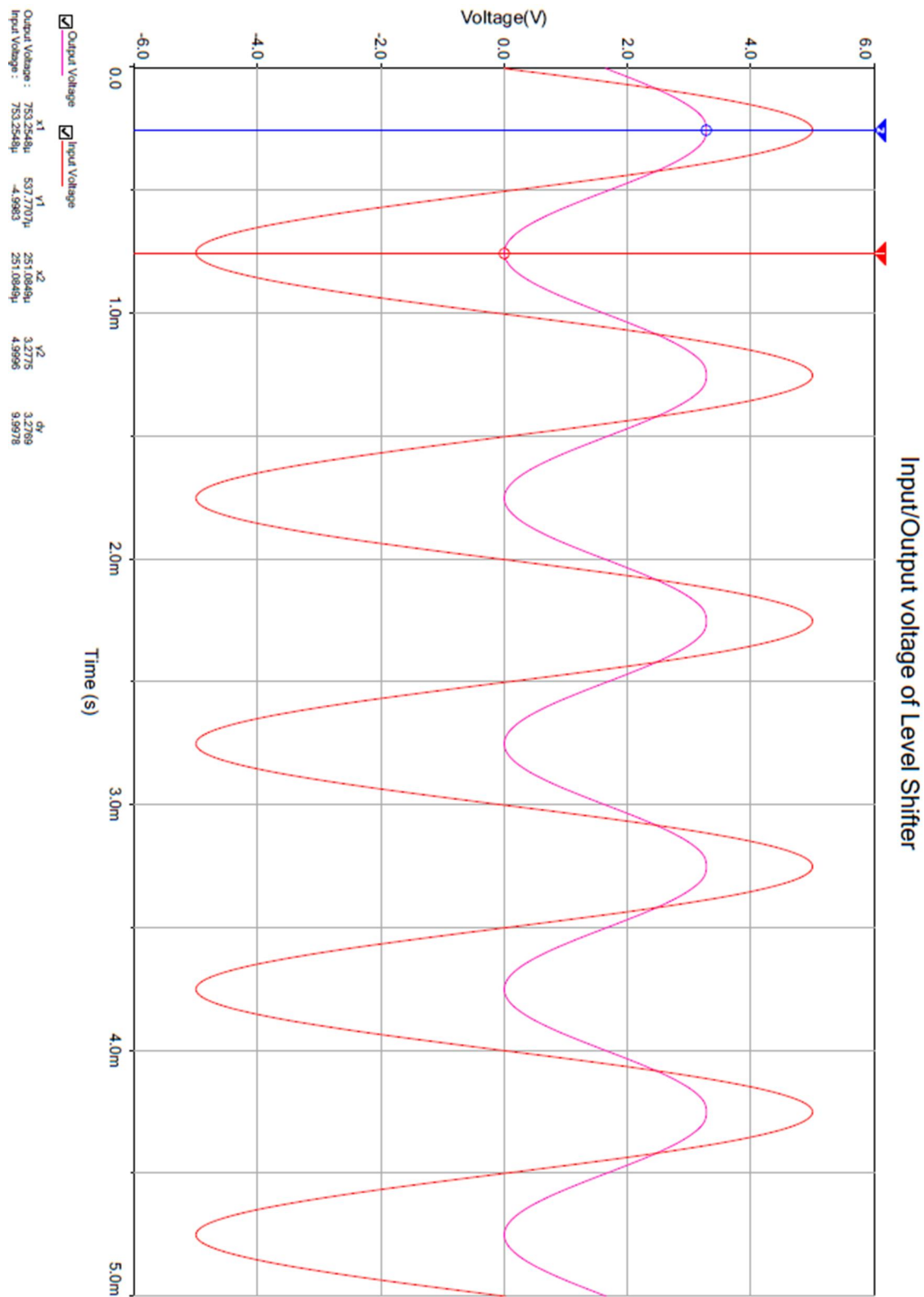
Frequency and Phase Response of Theoretical and Factual Low-pass Filter Simulation



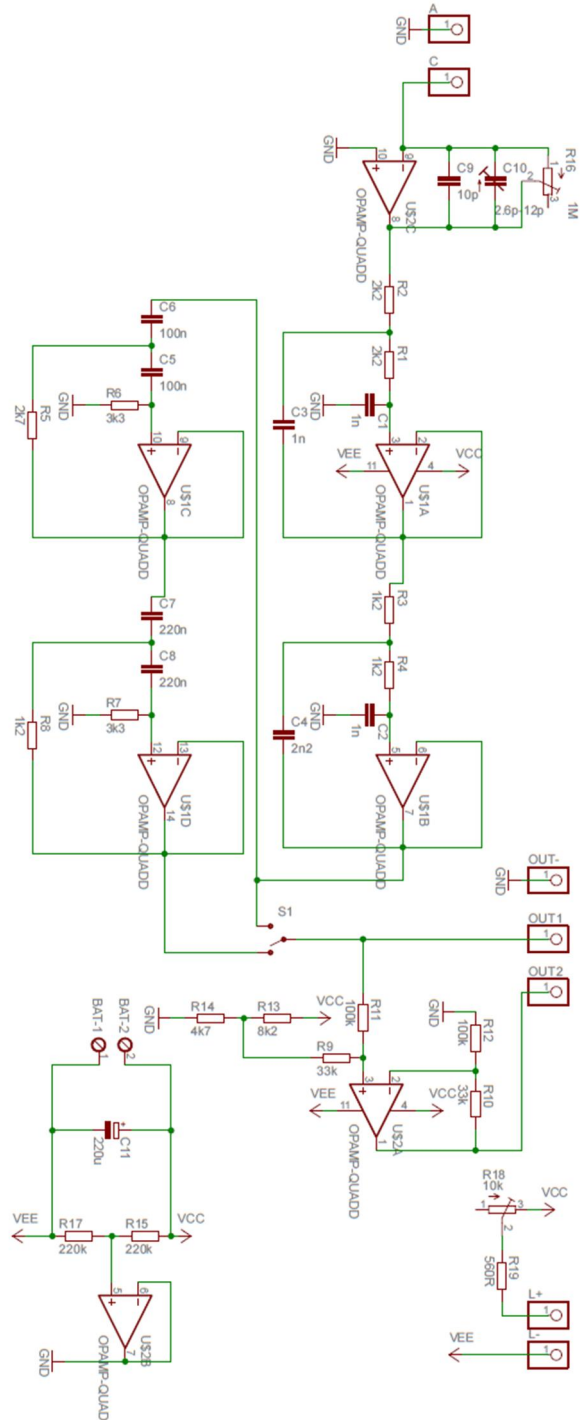
High-pass Filter frequency and phase response AC Analysis

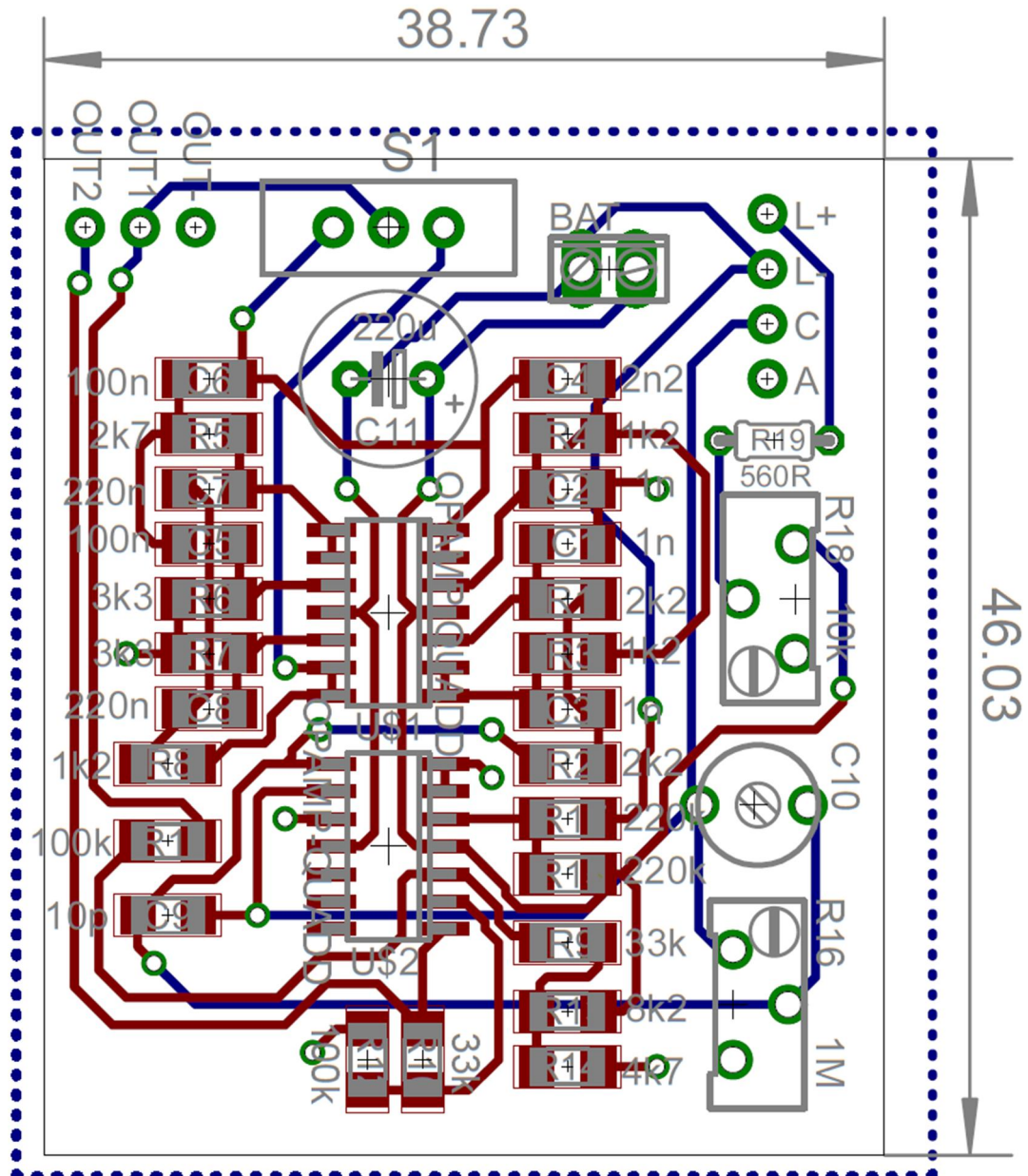
Frequency and Phase Response of Theoretical and Factual High-pass Filter Simulation



Input and Output Voltage of Simulated Level Shifter Circuit

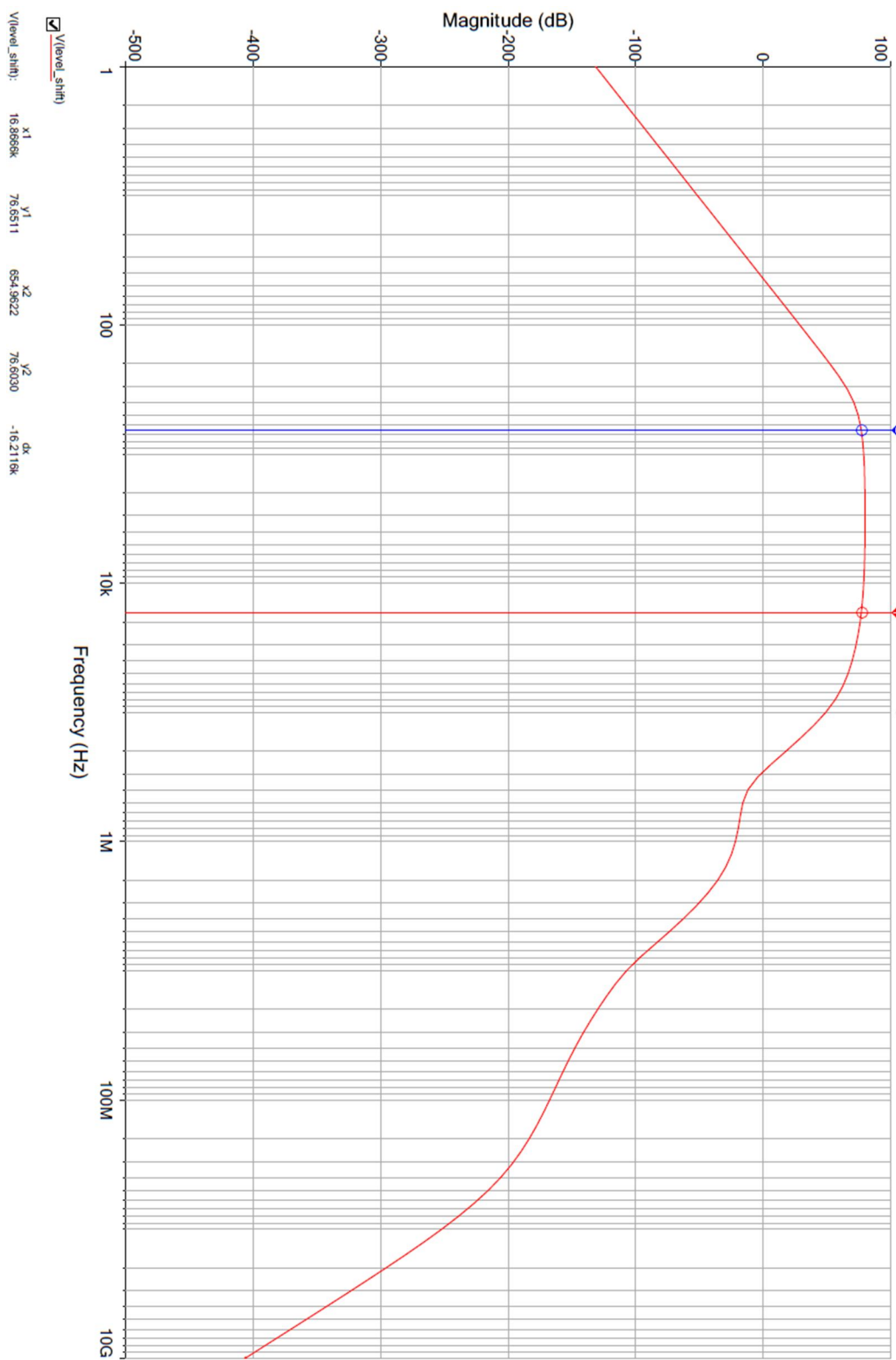
Circuit Diagram of the Main Board

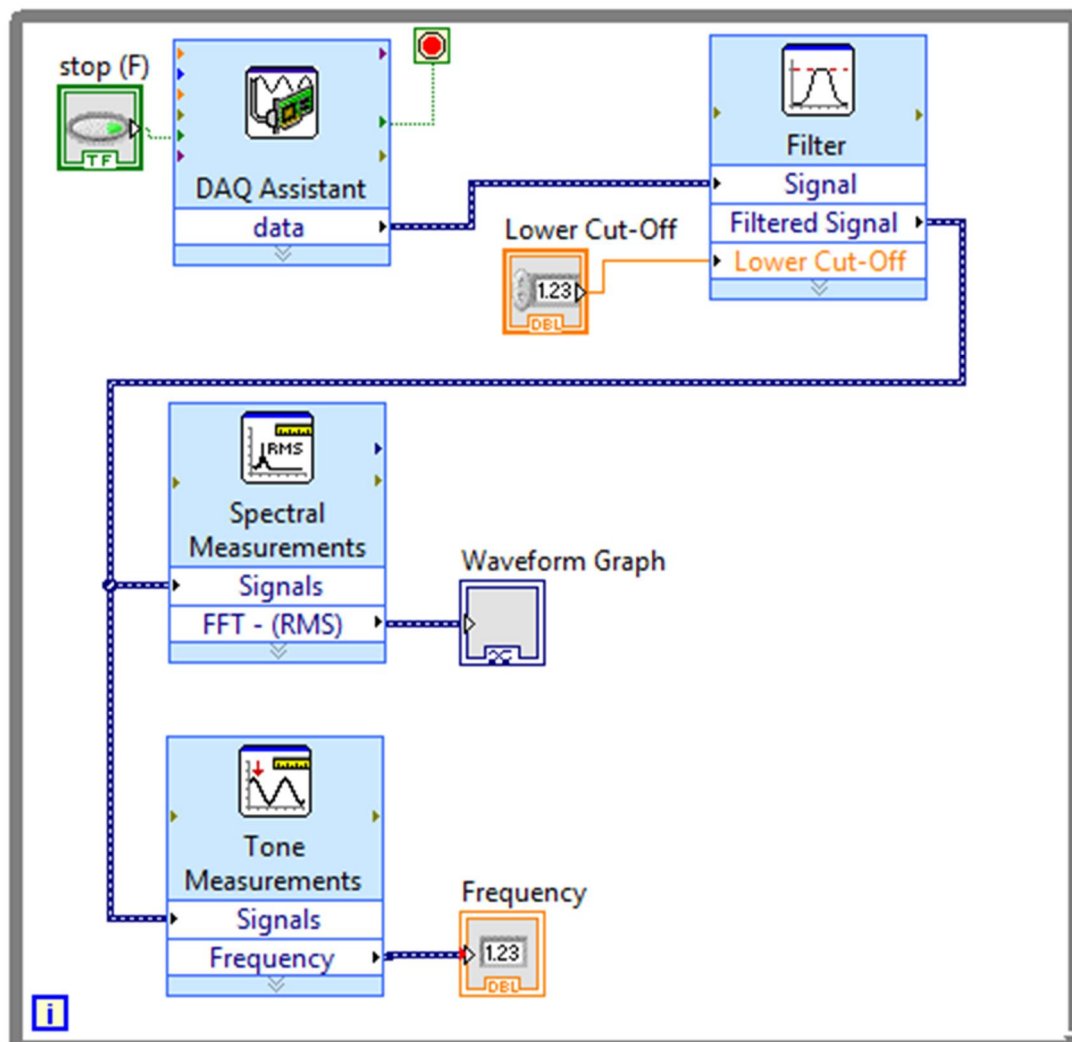


PCB Layout of the Main Board

Theoretical Frequency Response of the Whole Systems Simulation

Frequency Response of The Whole System
AC Analysis



Block Diagram of LabVIEW Program

Measurement Values of Figure 16

f (Hz)	U (V)
10,000	0,020
50,000	0,014
100,000	0,015
200,000	0,134
300,000	0,365
400,000	0,737
500,000	1,000
600,000	1,180
700,000	1,340
800,000	1,460
900,000	1,540
1000,000	1,600
2000,000	1,740
3000,000	1,760
4000,000	1,740
5000,000	1,700
6000,000	1,680
7000,000	1,640
8000,000	1,600
9000,000	1,540
10000,000	1,500
15000,000	1,260
20000,000	1,040
25000,000	0,841
30000,000	0,689
35000,000	0,569
40000,000	0,457
45000,000	0,377
50000,000	0,313
60000,000	0,209
70000,000	0,134
80000,000	0,092
90000,000	0,063
100000,000	0,049